U.S. Department
of Transportation
Federal Railroad
Administration

Office of Research,
Development and Technology
Washington, DC 20590

# Fire Performance of a Cryogenic ISO UN-T75 Storage Tank Using Analytical Methods and Fire Testing Phase 2: Testing with LNG in an ISO Tank

DOT/FRA/ORD-24-11

Final Report | February 2024

# REPORT DOCUMENTATION PAGE

*Form Approved*
*OMB No. 0704-0188*



| 1. AGENCY USE ONLY (Leave blank) | 2. REPORT DATE | 3. REPORT TYPE AND DATES COVERED |
|---|---|---|
| | October 24, 2023 | Final Report, 09/2016 to 08/2017 |

**4. TITLE AND SUBTITLE**
Fire Performance of a Cryogenic ISO UN-T75 Storage Tank Using Analytical Methods and Fire Testing, Phase 2: Testing with LNG in ISO Tank

**5. FUNDING NUMBERS**
693JJ622C000003

**6. AUTHOR(S)**
Jason Huczek – ORCiD: 0000-0002-2656-853X
Marc Janssens – ORCiD: 0000-0003-0088-4013
Kyle Fernandez – ORCiD: 0000-0003-2740-354X
Keith Friedman – ORCiD: 0000-0002-3133-4113
Garrett Mattos – ORCiD: 0000-0003-4682-7110

**7. PERFORMING ORGANIZATION NAME(S) AND ADDRESS(ES)**
Southwest Research Institute (SwRI)
6220 Culebra Road, Bldg. 143
San Antonio, TX 78238

Freidman Research Corporation (FRC)
1508-B Ferguson Lane
Austin, TX 78754

**8. PERFORMING ORGANIZATION REPORT NUMBER**
01.27392

**9. SPONSORING/MONITORING AGENCY NAME(S) AND ADDRESS(ES)**
U.S. Department of Transportation
Federal Railroad Administration
Office of Research and Development
Washington, DC 20590

**10. SPONSORING/MONITORING AGENCY REPORT NUMBER**
DOT/FRA/ORD-24-11

**11. SUPPLEMENTARY NOTES**
COR: Francisco González, III

**12a. DISTRIBUTION/AVAILABILITY STATEMENT**
This document is available to the public through the FRA Web site at http://www.fra.dot.gov.

**12b. DISTRIBUTION CODE**

**13. ABSTRACT (Maximum 200 words)**
FRA sponsored a study by Southwest Research Institute to conduct research and testing of a cryogenic storage tank in Liquefied Natural Gas (LNG) service and evaluate its thermal safety performance under fire conditions using analytical methods and fire testing. This report documents the second phase of this research. In Phase I, the team filled the test tank with liquid nitrogen (LN2) in place of LNG and the pressure relief system was evaluated and determined to work properly in the specified test conditions. Based on those results, researchers in Phase II essentially repeated the same test with the tank filled with LNG. The report provides additional detail of the test tank, the flatcar supporting the tank, the development of a safety plan, characterization of the fire exposure source, description of the instrumentation used in the experiment, test results, and detailed data analysis.

**14. SUBJECT TERMS**
Liquefied Natural Gas (LNG), Liquid Nitrogen (LN2), ISO UN-T75 Tank, Flatcar, Pressure Relief Valve/Device (PRV/PRD), Directional Flame Thermometer (DFT), Incident Heat Flux, Surface Temperature

**15. NUMBER OF PAGES**
69

**16. PRICE CODE**

| 17. SECURITY CLASSIFICATION OF REPORT | 18. SECURITY CLASSIFICATION OF THIS PAGE | 19. SECURITY CLASSIFICATION OF ABSTRACT | 20. LIMITATION OF ABSTRACT |
|---|---|---|---|
| Unclassified | Unclassified | Unclassified | |

**Standard Form 298** (Rev. 8/98)
Prescribed by ANSI Std. Z39.18

# METRIC/ENGLISH CONVERSION FACTORS

| ENGLISH TO METRIC | METRIC TO ENGLISH |
|---|---|
| **LENGTH (APPROXIMATE)** | **LENGTH (APPROXIMATE)** |
| 1 inch (in) = 2.5 centimeters (cm) | 1 millimeter (mm) = 0.04 inch (in) |
| 1 foot (ft) = 30 centimeters (cm) | 1 centimeter (cm) = 0.4 inch (in) |
| 1 yard (yd) = 0.9 meter (m) | 1 meter (m) = 3.3 feet (ft) |
| 1 mile (mi) = 1.6 kilometers (km) | 1 meter (m) = 1.1 yards (yd) |
| | 1 kilometer (km) = 0.6 mile (mi) |
| **AREA (APPROXIMATE)** | **AREA (APPROXIMATE)** |
| 1 square inch (sq in, $in^2$) = 6.5 square centimeters ($cm^2$) | 1 square centimeter ($cm^2$) = 0.16 square inch (sq in, $in^2$) |
| 1 square foot (sq ft, $ft^2$) = 0.09 square meter ($m^2$) | 1 square meter ($m^2$) = 1.2 square yards (sq yd, $yd^2$) |
| 1 square yard (sq yd, $yd^2$) = 0.8 square meter ($m^2$) | 1 square kilometer ($km^2$) = 0.4 square mile (sq mi, $mi^2$) |
| 1 square mile (sq mi, $mi^2$) = 2.6 square kilometers ($km^2$) | 10,000 square meters ($m^2$) = 1 hectare (ha) = 2.5 acres |
| 1 acre = 0.4 hectare (he) = 4,000 square meters ($m^2$) | |
| **MASS - WEIGHT (APPROXIMATE)** | **MASS - WEIGHT (APPROXIMATE)** |
| 1 ounce (oz) = 28 grams (gm) | 1 gram (gm) = 0.036 ounce (oz) |
| 1 pound (lb) = 0.45 kilogram (kg) | 1 kilogram (kg) = 2.2 pounds (lb) |
| 1 short ton = 2,000 pounds (lb) = 0.9 tonne (t) | 1 tonne (t) = 1,000 kilograms (kg) = 1.1 short tons |
| **VOLUME (APPROXIMATE)** | **VOLUME (APPROXIMATE)** |
| 1 teaspoon (tsp) = 5 milliliters (ml) | 1 milliliter (ml) = 0.03 fluid ounce (fl oz) |
| 1 tablespoon (tbsp) = 15 milliliters (ml) | 1 liter (l) = 2.1 pints (pt) |
| 1 fluid ounce (fl oz) = 30 milliliters (ml) | 1 liter (l) = 1.06 quarts (qt) |
| 1 cup (c) = 0.24 liter (l) | 1 liter (l) = 0.26 gallon (gal) |
| 1 pint (pt) = 0.47 liter (l) | |
| 1 quart (qt) = 0.96 liter (l) | |
| 1 gallon (gal) = 3.8 liters (l) | |
| 1 cubic foot (cu ft, $ft^3$) = 0.03 cubic meter ($m^3$) | 1 cubic meter ($m^3$) = 36 cubic feet (cu ft, $ft^3$) |
| 1 cubic yard (cu yd, $yd^3$) = 0.76 cubic meter ($m^3$) | 1 cubic meter ($m^3$) = 1.3 cubic yards (cu yd, $yd^3$) |
| **TEMPERATURE (EXACT)** | **TEMPERATURE (EXACT)** |
| [(x-32)(5/9)] °F = y °C | [(9/5) y + 32] °C = x °F |

## QUICK INCH - CENTIMETER LENGTH CONVERSION

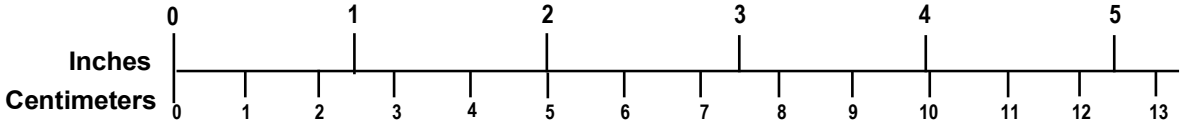


## QUICK FAHRENHEIT - CELSIUS TEMPERATURE CONVERSIO

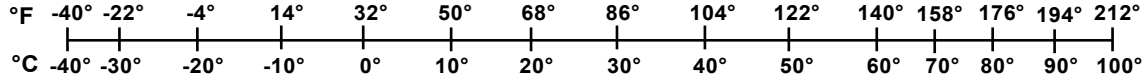


For more exact and or other conversion factors, see NIST Miscellaneous Publication 286, Units of Weights and Measures. Price $2.50 SD Catalog No. C13 10286

Updated 6/17/98

## Acknowledgements

Southwest Research Institute and Freidman Research Corporation acknowledge Francisco González III and Phani Raj at the Federal Railroad Administration for their technical guidance throughout this project.

## Contents

## Illustrations

## Tables

## Executive Summary

To realize potential reductions in Greenhouse Gas (GHG) emissions, fuel costs, and refueling times, the railroad industry is considering alternative fuels to diesel, including Liquefied Natural Gas (LNG) and Compressed Natural Gas (CNG). However, the safety performance of alternate-fuel tank cars under derailment-induced fire conditions has not been verified. To address this, the Federal Railroad Administration (FRA) sponsored a study by Southwest Research Institute to conduct research and testing of a cryogenic storage tank in LNG service and evaluate its thermal safety performance under fire conditions using analytical methods and fire testing.

This report documents the second phase of this research. In Phase I[1], the team filled the test tank with liquid nitrogen (LN2) in place of LNG and the pressure relief system was evaluated and determined to work properly in the specified test conditions. Based on those results, researchers in Phase II essentially repeated the same test with the tank filled with LNG.

Two different tender design approaches are under consideration by the Association of American Railroads Natural Gas Fuel Technical Advisory Group: 1) a tank car-based design based on the DOT 113 specification tank car; and 2) two 40-ft International Organization for Standardization (ISO) LNG containers back to back on a flat car. The team conducted fire testing on the second of these designs, a portable tank filled with LNG, located on top of a flat rail car, and exposed to a propane pool fire. Researchers fire-tested the tank car and demonstrated the performance of the pressure relief valve system installed on the tank. The pressure relief valves (PRVs) opened and were able to relieve the pressure in the tank fast enough to avoid a Boiling Liquid Expanding Vapor Explosion (BLEVE) event. In addition, several types of data were collected during the experiment to understand how fire exposure affects the internal and external heating of the tank.

The report provides additional detail of the test tank, the flatcar supporting the tank, the development of a safety plan, characterization of the fire exposure source, description of the instrumentation used in the experiment, test results, and detailed data analysis. This information may be used in future computer modeling efforts to predict performance with different tanks and fire scenarios.

[1] FRA Report No. DOT/FRA/ORD-20/02

# 1. Introduction

The Federal Rail Administration (FRA) sponsored Southwest Research Institute (SwRI) to conduct research and evaluate the fire performance of a cryogenic storage tank filled with Liquefied Natural Gas (LNG) using analytical methods and fire testing. This second phase of testing was conducted in June 2022.

## 1.1 Background

This report documents Phase 2 of the research study. In Phase I[2], the test tank was filed with liquid nitrogen (LN2) and the pressure relief system was evaluated and determined to work properly in the specified test conditions. Based on those results, the team essentially repeated the same test with the tank filled with LNG.

## 1.2 Objectives

The objective of this project was to conduct fire testing of an International Organization for Standardization (ISO) tank filled with LNG, located on top of a flat rail car, and exposed to a propane pool fire, and evaluate the pressure relief valve system.

## 1.3 Overall Approach and Scope

The team exposed a portable LNG tank for rail shipment to fire conditions and evaluated the performance of the pressure relief valve system. In addition, several types of data were collected during the experiment to understand how fire exposure affects the internal and external heating of the tank.

## 1.4 Organization of the Report

The report provides additional detail of the test tank and the flatcar supporting the tank (Section 2), development of a safety plan (Section 3), characterization of the fire exposure source and burning duration (Section 4), description of the instrumentation used in the experiment (Section 5), test results (Section 6), preliminary modeling calculations (Section 7), and research conclusions (Section 8).

[2] FRA Report No. DOT/FRA/ORD-20/02

# 2. Test Articles

The team used two primary test articles for this project, an ISO UN-T75 storage tank and a flat car supporting the tank. The following subsections provide additional details about these test articles.

## 2.1 LNG ISO Test Tank

An ISO UN-T75 storage tank, outfitted for LNG service, was procured from Cryogenic Vessel Alternatives (CVA)[3]. The tank's model number is CVA-12K-114-ISO and it measures 40 ft long, 8.5 ft high, and 8 ft wide. Figure 1 provides selected photographs of the tank used in this experiment. Additional figures may be referenced in Appendix A of this report.

**Figure 1. ISO Tank Photograph Prior to Testing (left: View from West; right: View from Northeast)**

Team members positioned a small propane burner and steel mesh wall approximately 15 ft from the tank end to ensure ignition of the PRV exhaust, prevent flashback, and improve visibility of the flame during testing.

On June 28, 2022, the test tank was filled with 9500 gallons of LNG by Airgas USA, LLC. This resulted in a starting fill level of nominally 78 percent. Additional details on the initial conditions of the LNG in the test tank are provided in Section 7 of this report.

## 2.2 Flatcar for ISO Tank Installation

Florida East Coast Railway (FECR) donated a flatcar for this project. This car consists of two connected cars. One of these cars was used for Phase I fire testing, and the second car was used in this Phase 2 testing. Figure 2 shows a photograph of the flatcar and the trucks at the remote test site.

[3] CVA was acquired by Taylor Wharton during the project.

**Figure 2. Flatcar Photographs (top: Flatcar Being Installed; bottom: Flatcar Trucks)**

# 3. Safety Plan Development

The team submitted a test plan that included technical details of the safety plan. The content of the plan for Phase 1 and Phase 2 was largely the same and was focused on designing the experiments to keep personnel safe. For Phase 1, the plan primarily centered on determining safe standoff distances for overpressure and exposure from the propane fires source, based on historical event data available at the time. The details of that analysis are not repeated in this report.

For Phase 2, the plan primarily focused on the change from LN2 to LNG and how it could impact the safety of personnel at the site. The primary hazard of interest was the possibility of a Boiling Liquid Expanding Vapor Explosion (BLEVE) and the plan confirmed the safe standoff distance required in the event of a BLEVE during the test. Additional details are provided below.

## 3.1 LNG vs LN2 in ISO Tank

Team member SwRI's Fire Technology Department (FTD) performed a fire test of an LNG cryogenic tank filled with LN2 and secured on top of a flat car on May 11, 2017, at SwRI's remote test site in Sabinal, Texas. Based on the successful performance of the pressure relief system in the first test, the team conducted testing with LNG at the same remote test site on June 28, 2022.

## 3.2 BLEVE Considerations

The FTD was supported by SwRI's Mechanical Engineering Division to estimate the likelihood and consequences of a BLEVE event given the test parameters.

The team determined that 1) a BLEVE event was considered unlikely provided the pressure relief valves (PRVs) on the portable tank operate as intended, but 2) in case the PRVs did not operate as intended, resulting in catastrophic tank failure, the personnel and data recording equipment at the test site should be located at a safe standoff distance (~450 m).

### *3.2.1 Potential for BLEVE*

Total potential energy released during BLEVE event defines the degree of hazard. However, BLEVE theory states that instantaneous nucleation and volumetric boiling of liquid content requires the temperature of the multiphase mixture be at or above the superheat limit temperature ($T_{sl}$) [1, 2]. For BLEVE events that move from the saturation curve to ambient pressure directly, the total mechanical energy release is substantially reduced [3, 4]. Figure 3 shows the saturation curve for methane (CH4) as well as the superheat limit temperature as a function of temperature and pressure. The pressures noted relate to the nominal operating pressures observed in Phase 1 testing and are labeled "SwRI Test Conditions." The region of the graph contained within the red, blue, and black dotted lines are the critical conditions for a BLEVE.

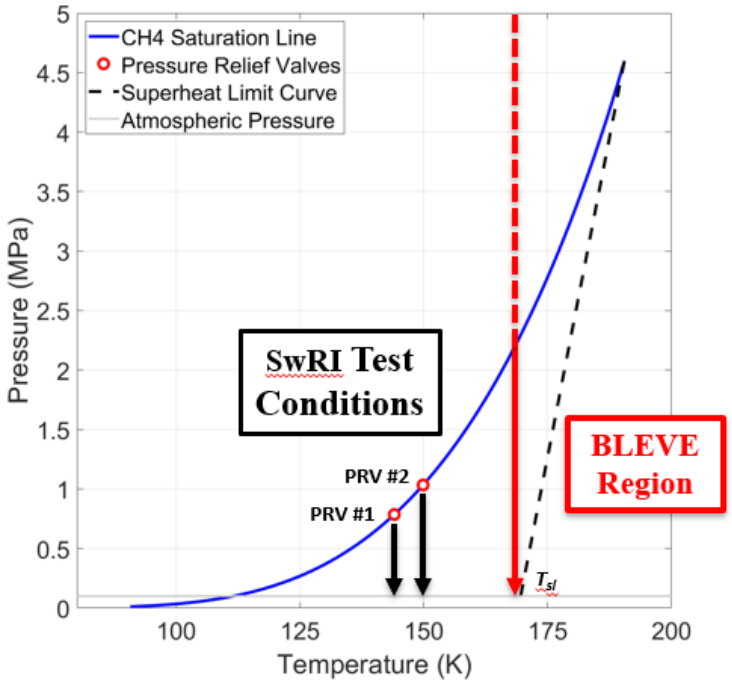


**Figure 3. BLEVE Conditions Illustrated on Methane Saturation Curve**

### *3.2.2 Energy Release Models*

The total energy release from the BLEVE is required to compute the blast overpressure. Several models exist for estimating BLEVE energy release. The team chose two models for this analysis:

- TNO Model (Modified by Birk) [5] – Assumes energy of blast wave is related to isentropic expansion work performed by expanding vapors
- Genova Model [6] – Relates mechanical expansion energy to thermal flashing of the liquid phase

After the total energy source for the blast wave is computed, Sach's scaling [7] is used to compute a blast overpressure at specified distances. Blast energy is used to compute dimensionless offset distance from the LNG vessel using Figure 4.

Table 1 provides a summary of the calculated energy source levels for varying fill percentages of the test tank. The energy levels calculated by the Birk model are substantially lower, but since it was not expected to experience volumetric flash boiling of the liquid phase (due to mixture temperatures being less than the superheat temperature limit), these may be reasonable estimates.

**Table 1. Summary of Calculated Energy Source Levels for BLEVE**

| LNG Fill Percentage | $E$ (Genova Model) - MJ | $\overline{E}$ (Birk TNO Model) - MJ |
|---|---|---|
| 84 | 123.7 | 3.6 |
| 50 | 73.7 | 11.2 |
| 25 | 36.8 | 16.8 |

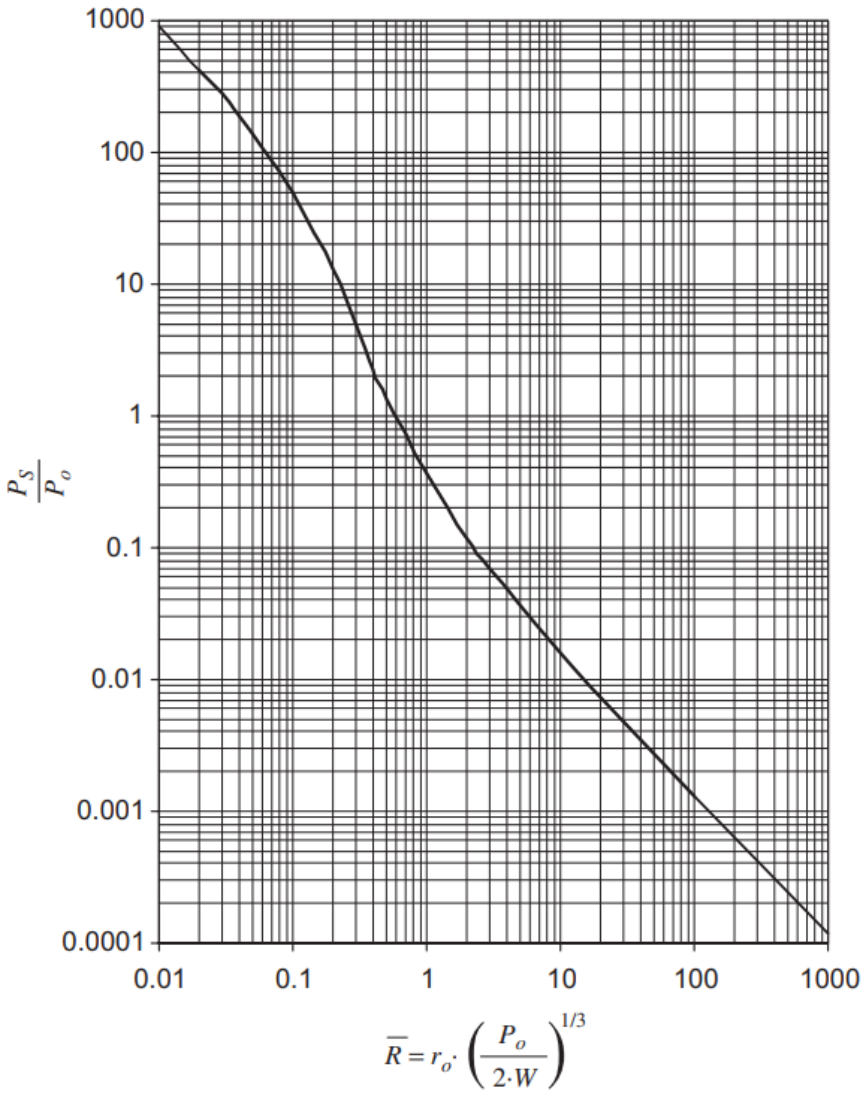


**Figure 4. Sach's Scaling: Scaled Overpressure vs. Scaled Distance for BLEVE Events**

Table 2 provides a summary of the calculated dimensionless offset distances per Sach's Scaling for five different distances (Figure 5 shows these results graphically).

**Table 2. Summary of Calculated Energy Source Levels for BLEVE**

| Distance (m) | $\overline{R}$ (Genova Model, 84%) | $\overline{R}$ (Birk TNO Model, 25%) |
|---|---|---|
| 100 | 9.4 | 18.2 |
| 200 | 18.7 | 36.4 |
| 300 | 28.1 | 54.6 |
| 400 | 37.4 | 72.8 |
| 500 | 46.8 | 91.0 |

The team made the following summary observations from this analysis:

- Using the Genova model, at 300 m, the shock overpressure is ≈ 500 Pa (0.07 psi)
- Using the Birk TNO model, at 300 m, the shock overpressure is ≈ 200 Pa (0.03 psi)

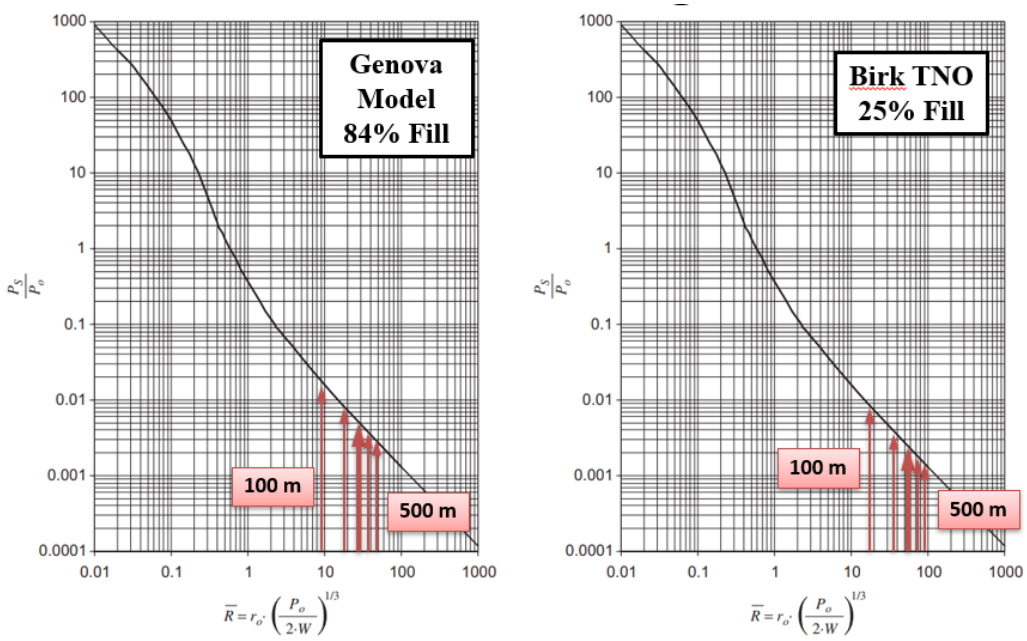


**Figure 5. Sach's Scaling Summary Results**

### *3.2.3 Location of Staff During Phase 2 Test*

Based on the calculations above, the location of the staff bunker during testing was located approximately 400 m from the test article and LNG source for the exposure fire. Figure 6 show these nominal locations at the remote test site. In each figure, the yellow highlighted box represents where the data collection and witnessing observers were located during the test.


**Figure 6. Location of Staff Bunker (yellow box) During Phase 2 Test (left: 408 m from Bunker to Propane Tank; right: 404 m from Bunker to Test Article)**

# 4. Characterization of Fire Exposure Source

The team considered a real accident scenario to determine the test duration. The following sections provide more detail about the assumed scenario, the calculated burning duration of the scenario (with safety factor) and the fire source to be used in the experiment for this duration.

## 4.1 Accident Scenario

The team considered an accident scenario in which a central ISO tank was exposed to an 18.3 × 6.1-m (60 × 20 ft) LNG spill/fire by two adjacent ISO tanks. Each ISO tank had a capacity of approximately 37,854 liters (10,000 gallons) of LNG. Therefore, the time was calculated for 75,708 liters (20,000 gallons) of LNG to evaporate (over a 20 s spill time) and burn (over the remainder of the calculated duration) based on literature values of published regression rates. This time was then used to calculate the required amount of liquid propane needed to provide exposure in testing.

## 4.2 Burning Duration Calculations

FRA provided a summary reference [8] on the topic of LNG regression rates in a series of large-scale experiments and recommended the rate to be used in this calculation.

The team sent a burning duration estimate [9] to FRA in December 2016 containing specific calculations and a summary of the input parameters used along with the relevant references for each input parameter. A safety factor of 2 was applied to the estimate based on earlier discussions with FRA. The team concluded that the maximum test duration would be approximately 73 min. The amount of propane required was calculated based on an exposure area of 12.2 × 3.1-m (40 × 10-ft) (i.e., nominal footprint of ISO tank on flatcar) for a test duration of 73 min.

Researchers amended the burning duration estimate [9] to include the required amount of propane to achieve the 73 min burning duration. The estimates, based on literature burning rates for propane [10], showed the required amount of propane for the experiment was approximately 30,283 liters (8000 gallons).

## 4.3 Fire Source Modifications

In Phase 1, the test burner consisted of a steel pan with a network of piping drilled with outlet holes for the liquid propane discharge. This piping was submerged at the start of the test under a layer of water, which was used to allow the liquid propane to evenly diffuse and form a pool fire under the flatcar and test tank.

Due to the intensity of the fire, it was not possible to maintain this water layer in the burner, and after approximately 60 min, the water was fully evaporated from the fire source. The water likely affected the heat transfer into the flatcar and test tank; since it was not possible to maintain the water layer, it is difficult to account for this in the data analysis.

For this reason, the team decided not to use water as the diffusion medium for the Phase II test. Instead, the liquid propane was allowed to flow into the test pan and gravel/stones were used as the diffusion medium.

In addition to the change in diffusion medium, the burner area was made 1 m wider. This was based on analysis from Phase 1 to maximum the heat input into the test tank.

Finally, additional structural supports were added under the flat car, within the fire burner. In Phase 1, the flatcar was observed to sag during the fire exposure, which can affect the heat transfer into the test article in a non-conservative way. For Phase 2, the team decided to provide additional support and delay or prevent the sagging of the flatcar during the test to maximize the heat input. Figure 7 shows a photograph of these additional supports.


**Figure 7. Structural Steel Pilons Installed to Support the Flatcar During the Test**

## 4.4 Final Fire Source Conditions

The fire source consisted of a 40 × 13-ft (i.e., nominal footprint of ISO tank on flatcar) LPG burner. A piping array was installed in the steel burner pan. The array comprised 8 branch lines and each branch line comprised 24 1/8-in. diameter holes.

The piping array was installed in the burner pan with the holes pointed downward, which allowed the LPG to diffuse evenly through the gravel layer contained in the burner pan. LPG was fed to the burner array at the Northwest and Southeast corners from a 2-in. buried pipe. An LPG supply system comprising an 8000 gal LPG tank, pump loop, and flow meter was setup approximately 300 m away from the test area.

An emergency stop button was routed to the control room to allow test personnel to safely stop the flow of LPG to the burner in case of an emergency.

Figure 8 shows a schematic of the Phase 2 burner construction and Figure 9 shows two photographs of the burner under construction and at final installation.

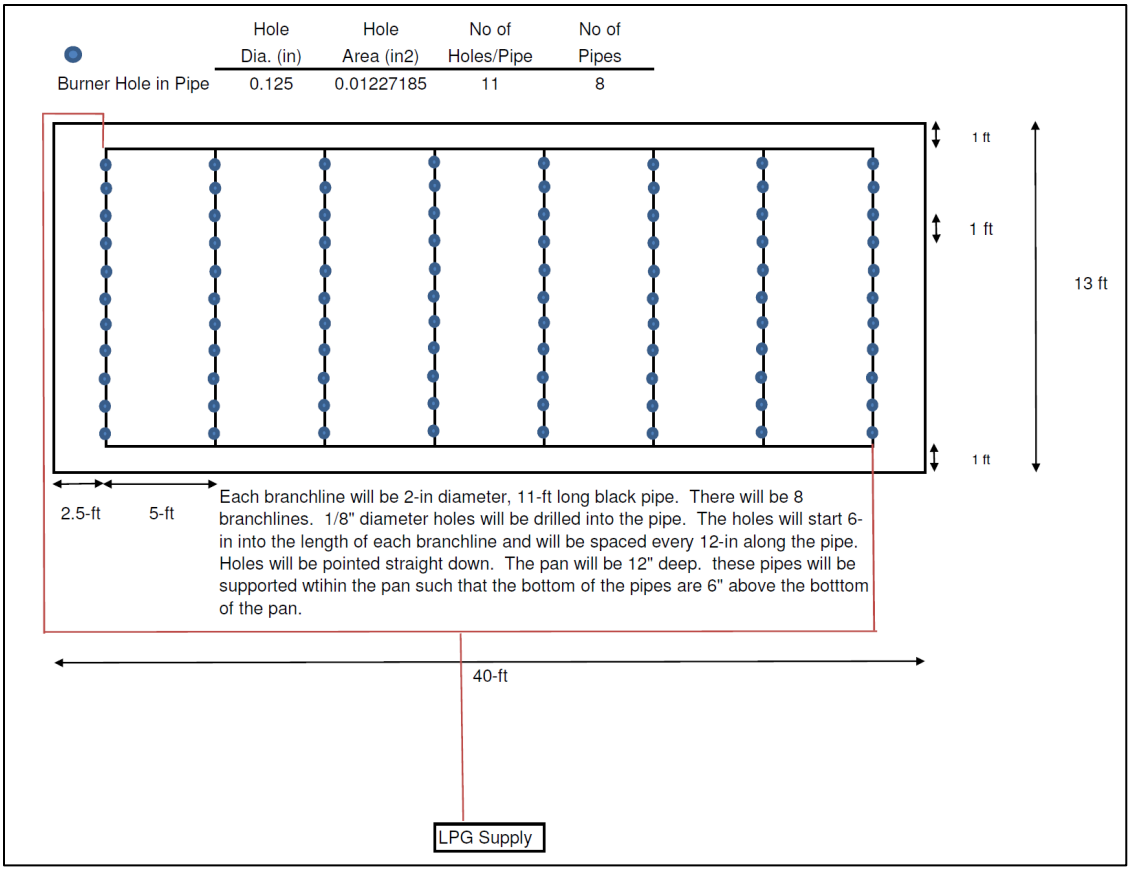


**Figure 8. Phase 2 Propane Test Burner Schematic**

**Figure 9. Phase 2 Propane Test Burner Photographs**

## 5. Test Instrumentation

Researchers used several types of instrumentation in this experiment. A total of 24 internal temperature measurements were taken, in addition to internal tank pressure, annular space vacuum pressure (between the inner and outer tanks), and pressure relief device (PRD) line pressure. Externally, 18 thermocouples (TCs) were provided around the tank and fire source to characterize the convective power of the fire and measure boundary layer temperatures. These are referred to as weld pad TCs in the test plan and Table 3.

An additional 18 TCs, referred to as directional flame thermometers (DFTs), were used to characterize the total heat flux from the fire and into the tank at several locations. Incident heat flux was measured at two targets (copper discs in Table 3) as well as blast pressure, in the event of a catastrophic failure. Finally, the liquid propane flow rate and the wind speed were measured. The test was also documented with high definition (HD) cameras from two stationary views and consumer drone video footage from two alternating drone cameras.

The team used two data acquisition systems (DAQs). DAQ 1 was used to collect the data from instruments closer to the test article. DAQ 2 was used to collect the data related to the LPG burner supply as well as the ambient temperature. Table 3 and Table 4 provide lists of the instrumentation and channel assignments used for each DAQ.

**Table 3. DAQ 1 Test Instrumentation List**

| Channel No. | Description* | DAQ ID |
|---|---|---|
| 1 | Center Float – Top – Large Probe | CF-T-LP |
| 2 | Center Float – Top – Medium Probe | CF-T-MP |
| 3 | Center Float – Top – Small Probe | CF-T-SP |
| 4 | Center Float – Bottom – Large Probe | CF-B-LP |
| 5 | Center Float – Bottom – Medium Probe | CF-B-MP |
| 6 | Center Float – Bottom – Small Probe | CF-B-SP |
| 7 | Shell Radial Float 1 | SRF-1 |
| 8 | Shell Radial Float 2 | SRF-2 |
| 9 | Head Radial Float 1 | HRF-1 |
| 10 | Head Radial Float 2 | HRF-2 |
| 11 | Zone A – Thermocouple 1 | A-TC1 |
| 12 | Zone A – Thermocouple 2 | A-TC2 |
| 13 | Zone A – Thermocouple 3 | A-TC3 |
| 14 | Zone A – Thermocouple 4 | A-TC4 |
| 15 | Zone B – Thermocouple 1 | B-TC1 |
| 16 | Zone B – Thermocouple 2 | B-TC2 |
| 17 | Zone B – Thermocouple 3 | B-TC3 |
| 18 | Zone B – Thermocouple 4 | B-TC4 |
| 19 | Zone B – Thermocouple 5 | B-TC5 |
| 20 | Zone B – Thermocouple 6 | B-TC6 |
| 21 | Zone C – Thermocouple 1 | C-TC1 |
| 23 | Zone C – Thermocouple 2 | C-TC2 |
| 24 | Zone C – Thermocouple 3 | C-TC3 |
| 25 | Zone C – Thermocouple 4 | C-TC4 |
| 27 | Weld Pad - West side of tank – North end of tank – center temp | WP-W-N-C |
| 28 | Weld Pad - West side of tank – Center of tank – center temp | WP-W-C-C |
| 29 | Weld Pad - West side of tank – South end of tank – center temp | WP-W-S-C |
| 32 | Weld Pad - East side of tank – North end of tank – center temp | WP-E-N-C |

| Channel No. | Description* | DAQ ID |
|---|---|---|
| 33 | Weld Pad - East side of tank – Center of tank – center temp | WP-E-C-C |
| 34 | Weld Pad - East side of tank – South end of tank – center temp | WP-E-S-C |
| 35 | West Tank Side – North differential flame thermometer – fire | WTS-N-DFT-F |
| 36 | West Tank Side – North differential flame thermometer – tank | WTS-N-DFT-T |
| 37 | West Tank Side – center differential flame thermometer – fire | WTS-C-DFT-F |
| 38 | West Tank Side – center differential flame thermometer – tank | WTS-C-DFT-T |
| 39 | West Tank Side – South differential flame thermometer – fire | WTS-S-DFT-F |
| 40 | West Tank Side – South differential flame thermometer – tank | WTS-S-DFT-T |
| 41 | East Tank Side – South differential flame thermometer – fire | ETS-S-DFT-F |
| 42 | East Tank Side – South differential flame thermometer – tank | ETS-S-DFT-T |
| 43 | East Tank Side – center differential flame thermometer – fire | ETS-C-DFT-F |
| 44 | East Tank Side – center differential flame thermometer – tank | ETS-C-DFT-T |
| 45 | East Tank Side – North differential flame thermometer – fire | ETS-N-DFT-F |
| 46 | East Tank Side – North differential flame thermometer - tank | ETS-N-DFT-T |
| 47 | North – fire source differential flame thermometer – fire | N-FS-DFT-F |
| 48 | North – fire source differential flame thermometer – tank | N-FS-DFT-T |
| 49 | North – fire source gas temperature | N-FS-GT |
| 50 | Center – fire source differential flame thermometer – fire | C-FS-DFT-F |
| 51 | Center – fire source differential flame thermometer – tank | C-FS-DFT-T |
| 52 | Center – fire source gas temperature | C-FS-GT |
| 53 | South – fire source differential flame thermometer – fire | S-FS-DFT-F |
| 54 | South – fire source differential flame thermometer – tank | S-FS-DFT-T |
| 55 | South – fire source gas temperature | S-FS-GT |
| 56 | Copper disc for incident heat flux – 75 ft. North – Bead | CD-N-B |
| 57 | Copper disc for incident heat flux – 75 ft. North – Disc | CD-N-D |
| 58 | Copper disc for incident heat flux – 75 ft. West – Bead | CD-W-B |
| 59 | Copper disc for incident heat flux –75 ft. West– Disc | CD-W-D |
| 60 | Weld Pad - West side of tank – North end of tank – top temp | WP-W-N-T |
| 61 | Weld Pad - West side of tank – North end of tank – bottom temp | WP-W-N-B |
| 62 | Weld Pad - West side of tank – Center of tank – top temp | WP-W-C-T |
| 63 | Weld Pad - West side of tank – Center of tank – bottom temp | WP-W-C-B |
| 64 | Weld Pad - West side of tank – South end of tank – top temp | WP-W-S-T |
| 65 | Weld Pad - West side of tank – South end of tank – bottom temp | WP-W-S-B |
| 66 | Weld Pad - East side of tank – North end of tank – top temp | WP-E-N-T |
| 67 | Weld Pad - East side of tank – North end of tank – bottom temp | WP-E-N-B |
| 68 | Weld Pad - East side of tank – Center of tank – top temp | WP-E-C-T |
| 69 | Weld Pad - East side of tank – Center of tank – bottom temp | WP-E-C-B |
| 70 | Weld Pad - East side of tank – South end of tank – top temp | WP-E-S-T |
| 71 | Weld Pad - East side of tank – South end of tank – bottom temp | WP-E-S-B |
| 72 | Pressure relief valve discharge pressure | PRV-P |
| 73 | Internal Tank Pressure | IT-P |

*Non-fire source DFTs – Back = Tank Side; Front = Fire Side; Fire Source DFTs – Back = Tank Side; Front = Fire Side; Copper Discs – Front = Exposed Copper Disc, Back = Internal TC

**Table 4. DAQ 2 Test Instrumentation List**

| Channel No. | Description | DAQ ID |
|---|---|---|
| 1 | LPG Flow Rate | LPG-F |
| 2 | Liquid propane discharge pressure (FT 0-200 PSI) | LPG-P |
| 3 | LPG Density | LPG-D |
| 4 | LPG Temperature | LPG-T |
| 5 | Ambient Air Temperature | AMB-T |

## 5.1 Internal Instrumentation

The internal instrumentation configuration represented the largest change in the Phase 2 test setup. In Phase 1, the internal data was lost after approximately 40 minutes because the internal TCs were overheated in a short section of piping that was difficult to adequately protect with insulation.

Several design changes were made for Phase 2 to avoid this problem. First, the TC type was changed from Type T to Type K. Type T is more accurate at cryogenic temperatures but is less resistant to higher temperatures as the test tank is heated and the system temperatures increase. In addition, the TC insulation and sheathing were changed to perform better at elevated temperatures.

Internal instrumentation included the gas/liquid/surface temperatures measured inside the test tank, as well as the internal tank pressure, annular space tank pressure and LNG liquid level. The team worked with CVA and one of their vendors, Conax Technologies, to accommodate internal temperature measurements.

In Phase 1, the pass-through connectors were in the piping cabinet, which was a challenging area to protect, leading to TC failure due to fire exposure. For the Phase 2 test, CVA provided access for the routing of the interior TCs through the top middle part of the tank, which was a much better area to protect those connections from fire exposure.

Figure 10 and Figure 11 show the arrangement of interior instrumentation as discussed above. Figure 11 provides a detail for the center and radial floats. Figure 12 provides a detail of the exit position for the TCs. Figure 13 provides detail for additional internal TCs. These figures are also provided in Appendix B.

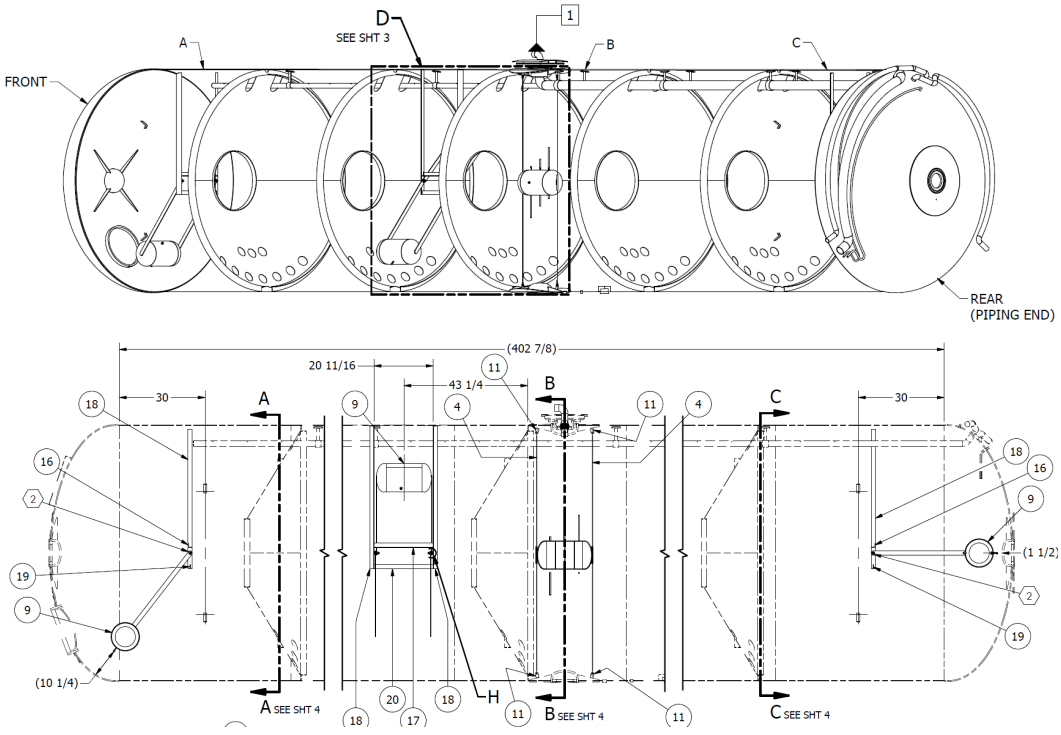


**Figure 10. Arrangement of Interior Thermocouples (provided by CVA)**

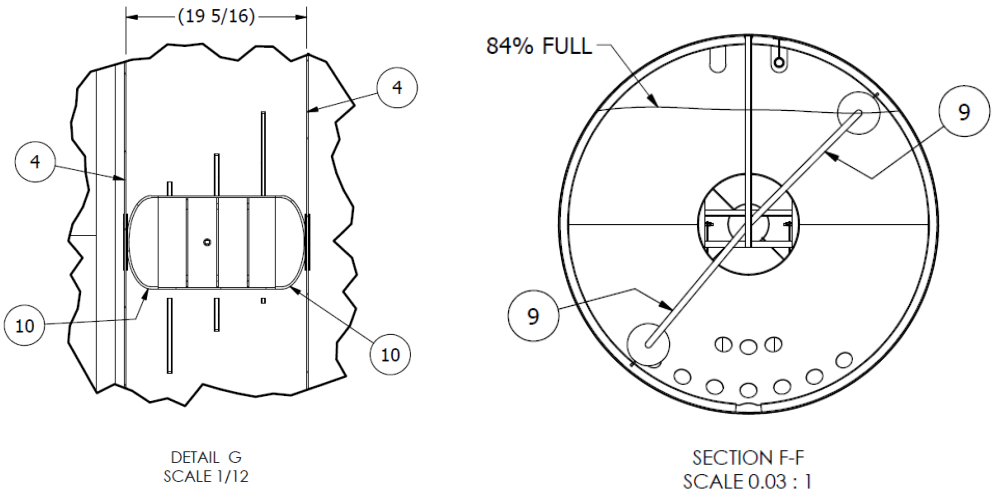


**Figure 11. Detail of Center Float as well as Shell Radial Floats (provided by CVA)**

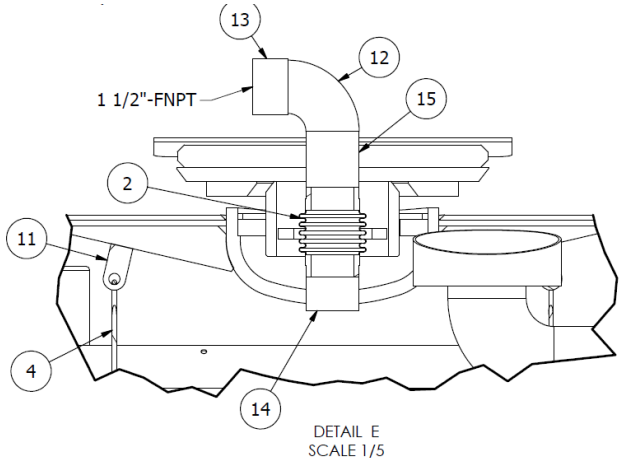


**Figure 12. Detail of Penetration Location for Exit of Thermocouples (provided by CVA)**

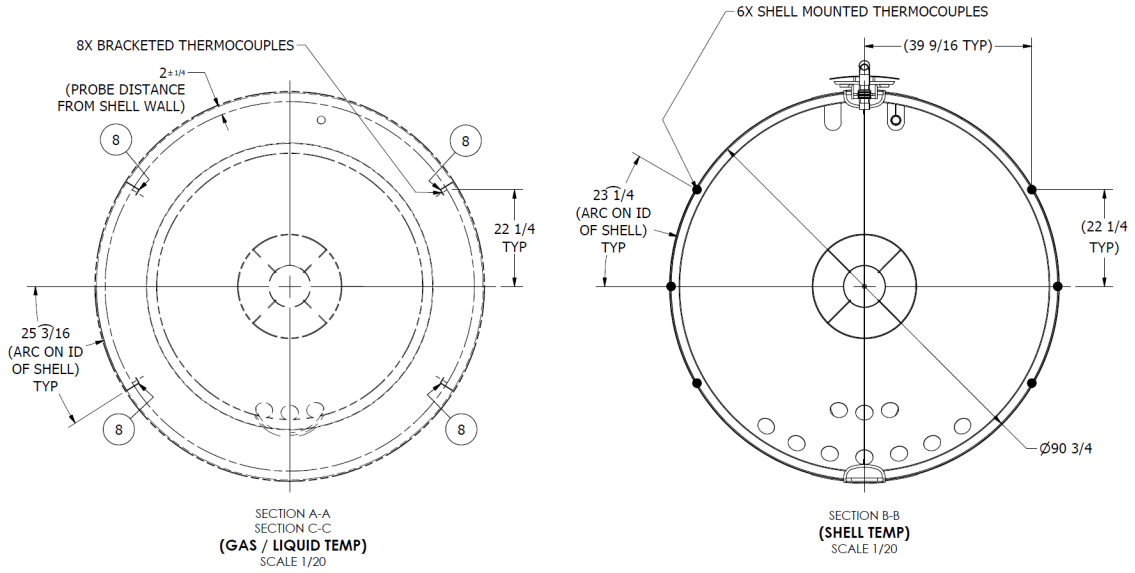


**Figure 13. Detail of Additional Internal Thermocouples (provided by CVA)**

In addition, researchers worked with CVA to measure the inner tank pressure, annular space (i.e., vacuum) pressure, and liquid level (the team ordered a separate meter from CVA to estimate the liquid level). Also, a second vacuum pressure port was added to the top of the tank where the internal TCs are routed out of the tank because it is an easier section of the tank to protect with insulation in a fire test.

## 5.2 External Instrumentation

The external instrumentation included TCs used to characterize the fire source intensity, the heat flux at the exterior of the test tank, and incident heat flux downrange to targets.

In addition to the thermal instrumentation described above, video and photographs were archived for review. A selected group of photographs are included in this report.

### *5.2.1 Directional Flame Thermometer*

The DFT was originally developed for measuring temperatures and heat fluxes in pool fires [11]. The DFT is conceptually like the plate thermometer but consists of two 3-mm thick, 120 × 120-mm Inconel plates with a 25-mm thick ceramic fiber blanket in between (see Figure 14). The blanket is compressed to 19-mm thickness. A 1.6-mm diameter sheathed Type K TC with insulated junction is in a groove on the inside of each plate.

An advantage of the DFT over the plate thermometer is that the heat transfer through a DFT can be calculated with an inverse heat transfer code such as IHCP1D [12]. The use of these devices in fire experiments has been standardized recently in ASTM E3057 [13].

**Figure 14. Directional Flame Thermometer**

### *5.2.2 Weld-Pad Surface Temperature Thermocouple Probe*

The Weld-Pad Surface Temperature Thermocouple Probe is designed for use in industrial applications to measure surface temperature by way of weld, braze, or clamp attachment. The pad is flexible to form to the contour of a flat or curved surface. The pad material is 304 stainless steel and measures 1.0 × 1.0 × 0.01 in. (25-mm × 25-mm × 0.25 mm) and the TC is Type K. Figure 15 shows a photograph of one of the weld-pad TCs.

**Figure 15. Weld-Pad Surface Temperature Thermocouple Probe**

### *5.2.3 Copper Disc Calorimeter*

Incident heat flux downrange was calculated from the response of a custom designed copper disk calorimeter. The sensor comprises a thin copper disc, approximately 0.3-mm (12 mil) thick and 13-mm (1/2-in.) diameter. The chromel and alumel wires of a 24 AWG type K TC are silver soldered to the back side of the disc. The TC wires are then pulled through small holes and taped to the backside of a 13-mm (1/2-in.) thick, 100 × 100 mm (4 × 4-in.) piece of ceramic fiber board (Unifrax Duraboard LD), so that the copper disc is in contact with the exposed surface of the ceramic fiberboard (see Figure 16). The exposed side of the copper disc and ceramic fiberboard are coated with a thin layer of black, heat-resistant paint with a known emissivity/absorptivity of 0.9 (Thurmalox® Solar Collector Coating, 250 Selective Black).

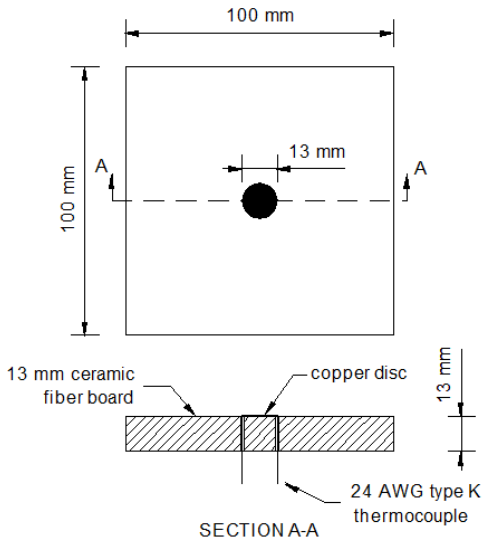


**Figure 16. Copper Disc Calorimeter**

The ceramic fiber board is backed by a 13-mm (1/2-in.) thick calcium silicate substrate, which is backed by a 25-mm (1-in.) thick layer of ceramic fiber blanket. All these materials are housed in a small metal enclosure measuring 100 × 100 × 50 mm deep (4 × 4 × 2 in. deep). The housing and additional substrates are not pictured.

### 5.2.4 General Instrumentation Layout Sketch

Figure 17 provides a plan view general layout of the external instrumentation at the remote site. Figure 18 provides a sketch of the additional weld-pad TCs that were added to obtain additional model validation data. Note that the fire source differential flame thermometers depicted in red were located between the fire source and underside of the flatcar. The differential flame thermometers depicted in green were located approximately 2 in. from the outer tank wall at the same nominal location as the weld-pad TCs and internal TCs at the same baffle position.

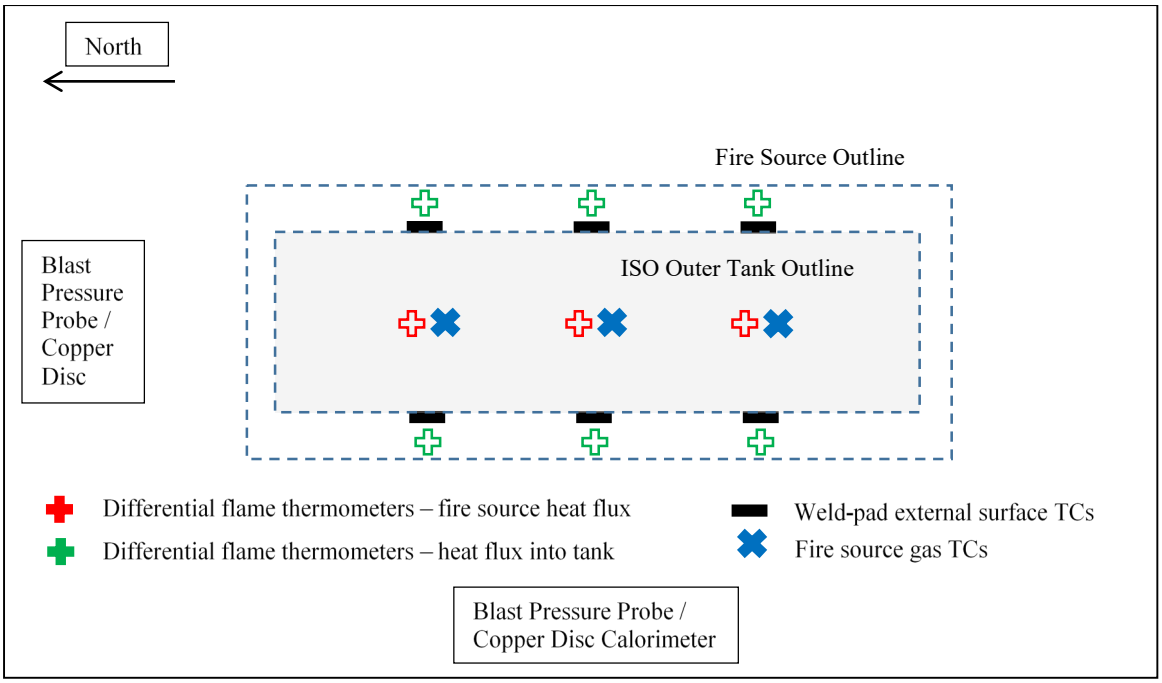


**Figure 17. External Instrumentation Sketch**

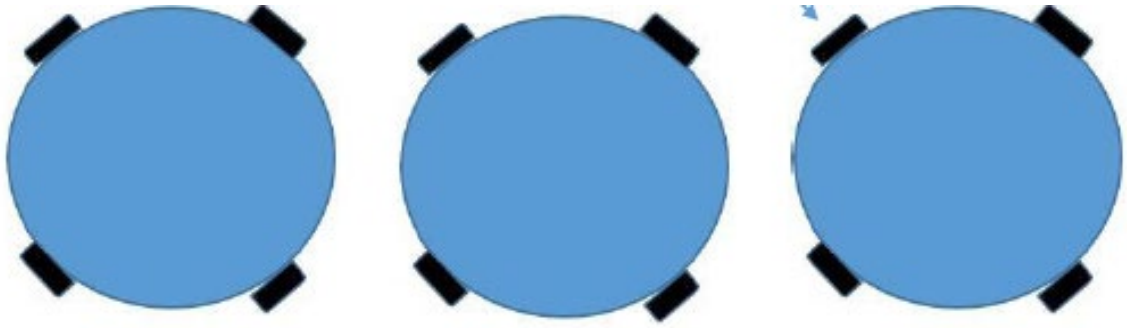

**Figure 18. Additional Weld-Pad Surface TCs Nominal Locations (Elevation View)**

Figure 19 provides a similar plan view with distances to cameras and instrumentation. Figure 20 and Figure 21 provide elevation view details of the location of weld-pad TCs and DFTs. The additional Weld-Pad TCs that are shown schematically in Figure 18 were installed approximately 17 in. below and 24 in. above the centerline positions shown in Figure 20. These dimensions are not shown on Figure 20 for clarity of viewing.

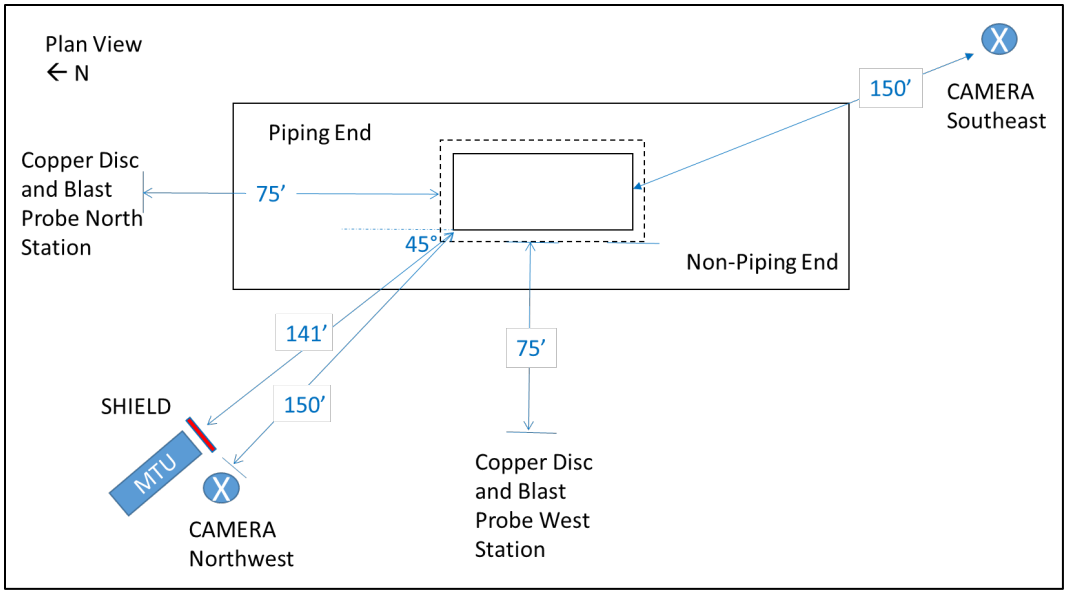


**Figure 19. External Instrumentation Sketch (Nominal Distances to Cameras and Instrumentation)**

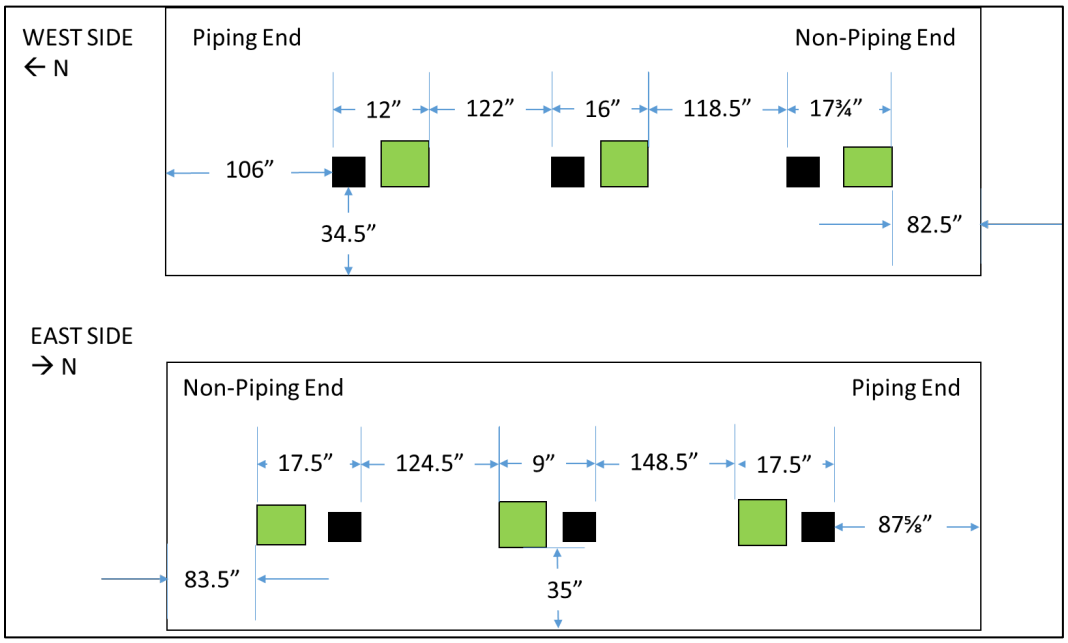


**Figure 20. Centerline Weld-Pad TCs (black squares) and DFT Locations (green squares) – Elevation View from the East and West**

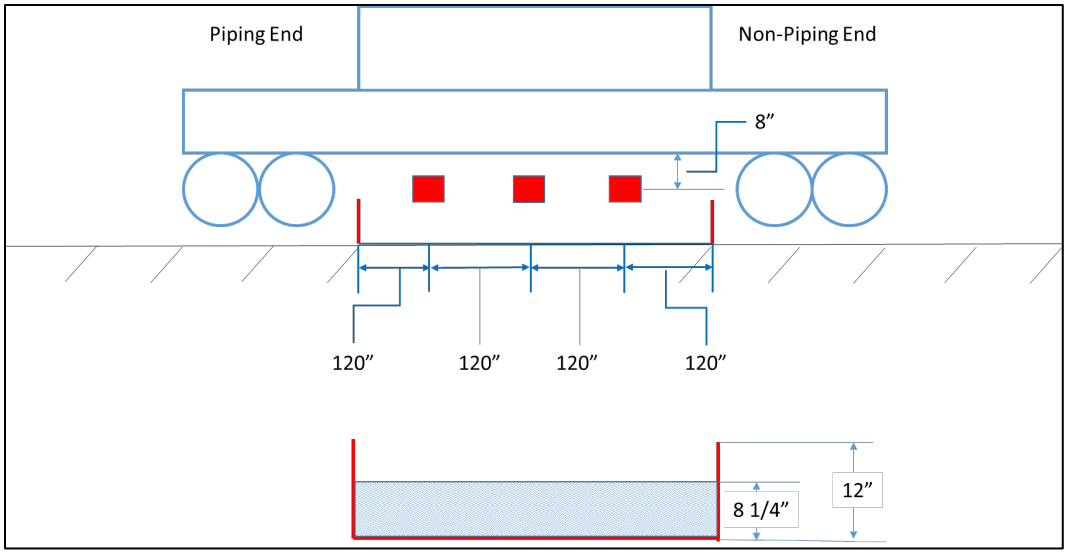


**Figure 21. Fire Source DFT Locations (red squares) and Burner Pan Dimensions (Elevation View)**

### *5.2.5 Drone Video Footage of Phase 2 Fire Test*

The team opted to incorporate drone video footage into Phase 2. The team used multiple drones and battery packs so that a second drone could be deployed immediately after the return of the first drone to ensure more continuous footage. After the drone returned to base, the battery was replaced, memory card checked for available space, and the drone prepared to re-deploy when necessary. Figure 22 shows a still shot from one of the drones during checkout tests of the test tank installed at the remote test location.

**Figure 22. Drone Footage Still Shot of Test Tank and DAQ Location**

# 6. Test Results

The team worked with SwRI's Fire Technology Department to perform a fire test of an LNG cryogenic tank secured on top of a flat car on June 28, 2022, at SwRI's remote test site in Sabinal, Texas.

The tank was exposed to the external LPG fire source for approximately 56 min. Table 5 summarizes the test observations. Figure 26 – Figure 31 provide the data from the test for the first 3.5 h. Selected post-test data is provided in Figure 32 – Figure 34.

The tank safely vented its contents and did not rupture, so no blast pressure data was collected or included in the instrumentation list.

The following sections provide selected photographs of the setup, testing, and post-test conditions, a summary of the video observations, a summary of the test data, and post-test observations and recommendations.

## 6.1 Selected Photographs

Figure 23 – Figure 25 show the test setup and pre- and post-test condition of the tank.

**LPG Supply Tank, Pump and Bypass**

**PG Flow Meter**

**Container Control Room**

**ISO Tank (east side)**

**ISO Tank (west side)**

**ISO Tank (north side)**

ISO Tank (South Side)

Instrumentation Trailer (NW of ISO Tank)

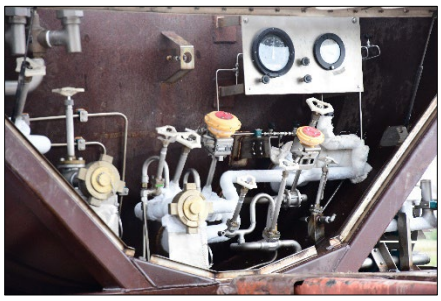

Valve Cabinet

Valve Cabinet

**Figure 23. Selected Setup and Pre-Test Photographs**

Test in Progress (view from east side)

Test in Progress (view from west side)

Test in Progress (PRV operating)

Test in Progress (PRV operating)

**Figure 24. Selected Testing Photographs**

Post-Test: ISO Tank (east side)

Post-Test: ISO Tank (west side)

Post-Test: ISO Tank (north side)

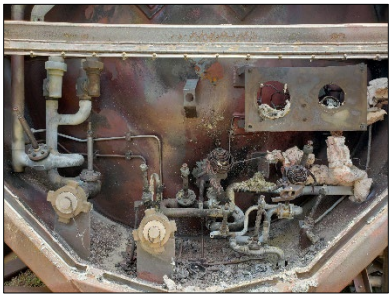

Post-Test: Close-Up of Valve Cabinet

**Figure 25. Selected Post-Test Photographs**

## 6.2 Video Observations

Table 5 summarizes the observations recorded during the test. The data acquisition system was started approximately 21 min and 50 s prior to burner ignition based on when the PRD actuation synchronized with the video.

**Table 5. Test Observations**

| Time (h:min:s) | Observations |
|---|---|
| -15:00:00 | Tank is filled with LNG |
| 00:00:00 | Ignition of propane burner under flatcar (7:34 am on June 29, 2022) |
| 00:02:40 | Vacuum pressure increased to 200 mTorr (initially at ~35 mTorr) |
| 00:04:00 | Vacuum pressure increased to 1100 mTorr (maximum of meter range) and stayed at this value for duration of test |
| 00:06:30 | Noticeable deformation beginning on east side of tank external jacket |
| 00:23:40 | Internal tank pressure increased to 75 psig (initially at ~45 psig) |
| 00:29:12 | Internal tank pressure increased to 100 psig |
| 00:32:00 | Internal tank pressure increased to 114 psig (PRD setting) |
| 00:32:22 | Activation of PRD and ignition of LNG jet flame ~1 s later |
| 00:32:45 | PRD reset (closed); jet flame extinguished |

| Time (h:min:s) | Observations |
|---|---|
| 00:33:19 | PRD open; jet flame ignited |
| 00:33:43 | PRD reset; jet flame extinguished |
| 00:34:03 | PRD open; jet flame ignited |
| 00:48:16 | The liquid propane source was shut off due to the internal tank pressure (160 psig) rising fast to a value that was deemed detrimental to the structural integrity of the internal tank. The internal pressure peaked at ~180 psig, before starting to decrease after fire exposure terminated. |
| 00:53:30 | Burner flames reduced to roughly 50% their nominal size |
| 00:54:30 | Burner flames reduced to roughly 10% of their nominal size |
| 00:56:10 | Residual propane exposure fire self-extinguished after consuming all the remaining propane in the supply line and burner pan |
| 00:56:30 | Frost visible on external tank (east side) |
| 01:12:19 | First indication of flames within the piping cabinet/tank end |
| 01:25:00 | Fire engulfs entire piping cabinet end |
| 01:30:00 – 03:30:00 | Continued venting of test article, including substantial fire in piping cabinet leading to likely failure of mechanical fitting connections and possibly affecting internal tank pressure measurement |
| 03:30:00 | Data file stopped and new file started within a few seconds to begin logging post-test data of internal temperatures and pressure (10:44 am on June 29, 2022) |
| 09:57:00 | Internal tank pressure decreased to 6-8 psig, data file stopped, and another file started to collect data overnight (3:11 p.m. on June 29, 2022) |
| 26:00:00 | Approximately 9:30 am on June 30, 2022 – internal tank pressure decreased to ~3-6 psig and cabinet fire size visually decreased compared to previous day |
| 32:30:00 | Approximately 4 pm on June 30, 2022 – internal tank pressure decreased to ~1-4 psig, cabinet fire still burning, but intensity continuing to decrease |
| Post-test | Internal tank temperatures and pressure continued to be monitored intermittently until fire burned out after approximately 48 h. After cabinet fire was out and tank had cooled to nominal ambient conditions, the tank was purged with nitrogen before arrangements were made to transport the tank back to SwRI's main campus and complete the cleanup activities offsite. |

## 6.3 Data Summary

Figure 26 provides a summary of the temperature and heat flux data from the DFTs centrally located on each side of the tank and over the fire source. Figure 27 shows the incident heat flux data, as determined from the copper disc calorimeters. Figure 28 and Figure 29 show the internal tank temperatures in the center and the ends of the tank for the first few hours of the test. Figure 30 shows the internal pressure and level data in the tank over the first few hours of the test and Figure 31 shows the annular space pressure and pressure relief pipe pressure for the early part of the test. Figure 32 - Figure 34 show selected data over the extended post-test duration.

As seen in Figure 26, the fire exposure to the tank was not uniform likely due to wind conditions. This resulted in a more severe exposure on the east side of the tank compared to the west side. The peak incident heat flux to the east side of the tank was 225.2 kW/m$^2$ and the peak incident heat flux to the west side of the tank was 32.1 kW/m$^2$. The peak incident heat flux from the fire source to the bottom of the flatcar was 105.7 kW/m$^2$.

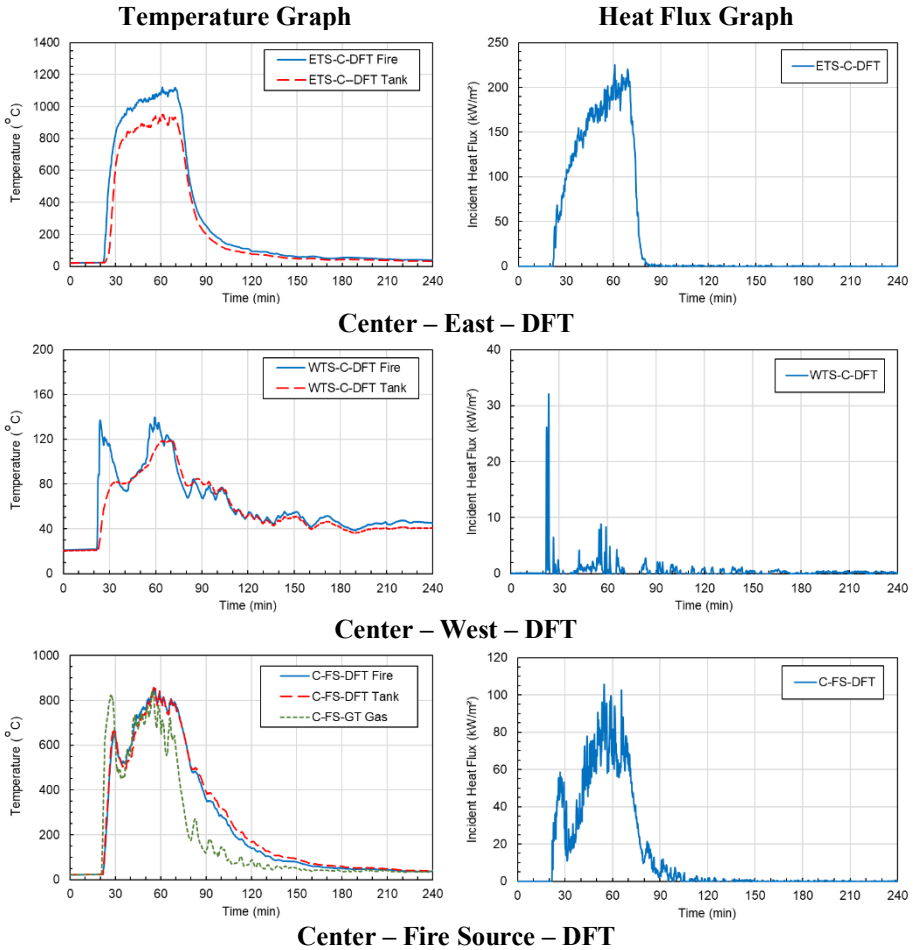


**Figure 26. Selected DFT Heat Flux Data**

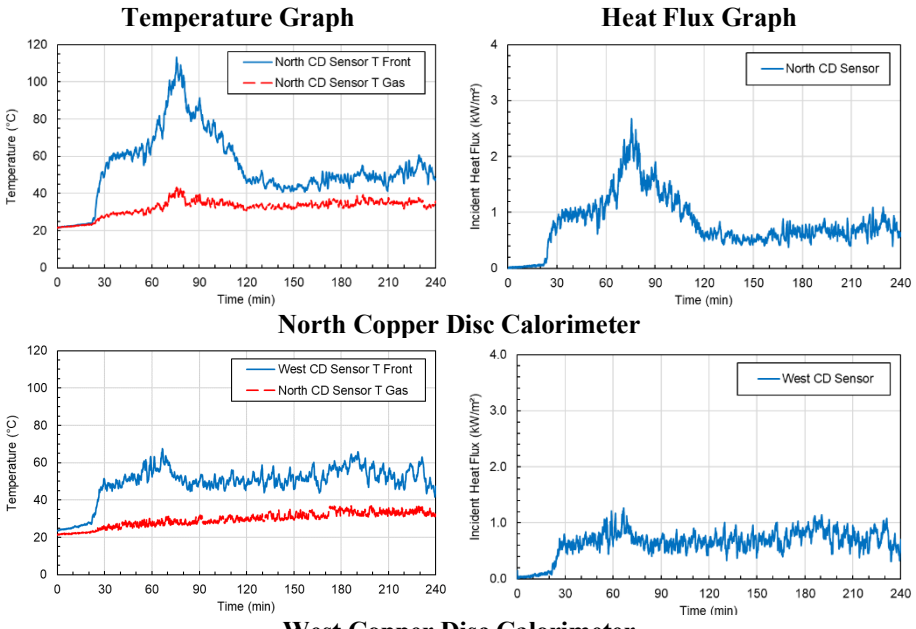


**Figure 27. Incident Heat Flux to Downfield Targets Data**

Figure 27 shows the incident heat flux to targets 23 m away in the north and west directions. The peak incident heat flux to these targets was relatively low; the peak in the north direction was 2.68 kW/m$^2$ and the peak in the west direction was 1.27 kW/m$^2$. It was likely higher in the north direction for a longer duration due to the continued burning in the valve cabinet area after the fire exposure was terminated. Unfortunately, no similar measurement was taken on the east side of the tank, which would have likely been the highest radiative heat flux due to the non-uniform exposure on the tank from the fire source due to the ambient wind conditions.

Figure 28 and Figure 29 show that the internal temperatures throughout the tank changed relatively consistently over the duration of the fire exposure. The internal temperature increased from approximately -215 °C to -165 °C.

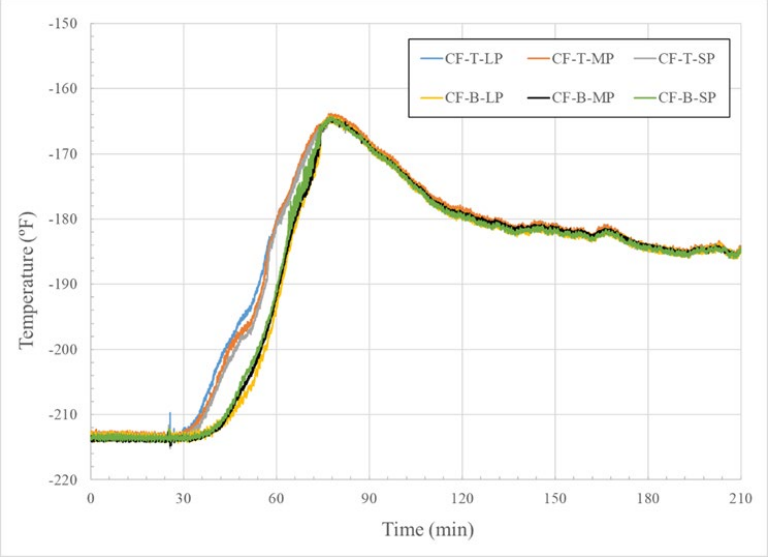


**Figure 28. Internal Temperatures in Center of Tank**

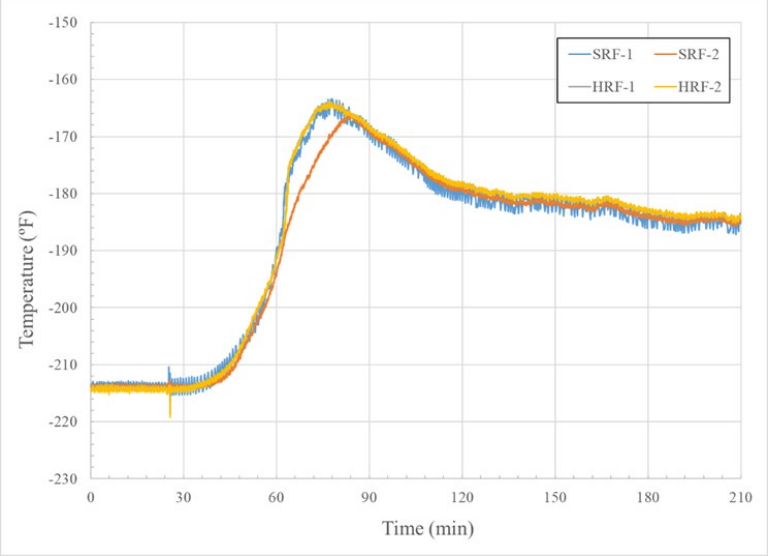


**Figure 29. Internal Temperatures at Ends of Tank**

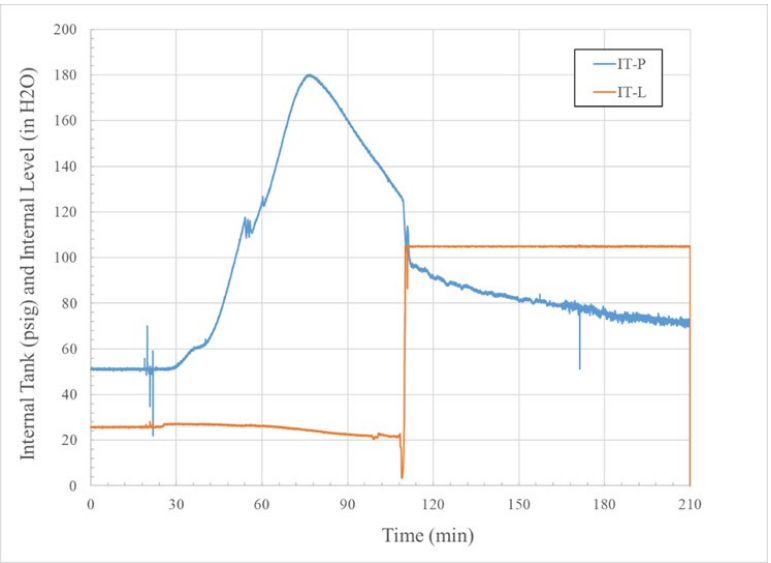


**Figure 30. Internal Tank Pressure and Level Data**

Figure 30 shows the internal tank pressure increase from 345 kPa (50 psig) to 1.24 MPa (180 psig) over the fire exposure duration. The tank liquid level was also measured during the test and reflected by the IT-L series in Figure 30. Unfortunately, after approximately 110 min, this signal was unreliable, likely due to overheating.

The pressure relief valves (PRVs) seemed to operate at the correct nominal pressure. As seen in Figure 31, the first large increase on the PRV-P channel occurred at an internal tank pressure of approximately 807 kPa (117 psig), which coincides with the stated set pressure of 793 kPa (115 psig). From this point in the test, the PRVs continued to open and close as necessary based on the internal pressure. Figure 31 also shows the annular space pressure between the inner and outer tank. Based on this data as well as the fast internal tank pressure rise during the fire exposure, it is likely the vacuum in the annular space was lost within a few minutes of fire exposure.

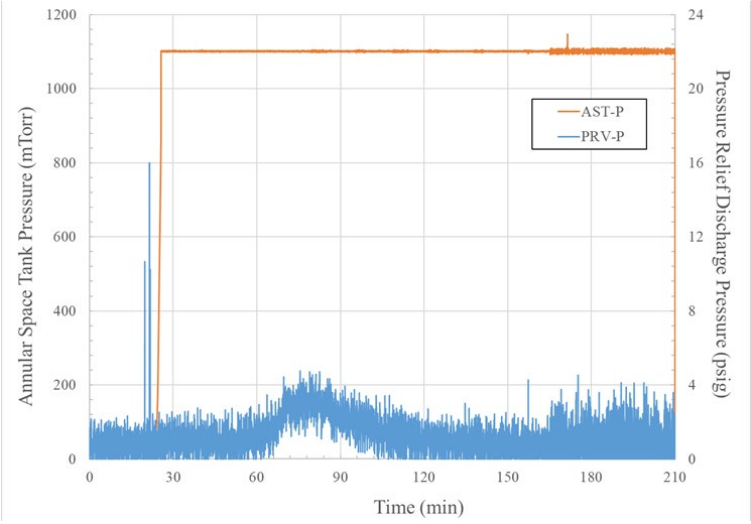


**Figure 31. Annular Space Pressure and Pressure Relief Discharge Pressure**

In Figure 32 - Figure 34, selected post-test data are presented to show how the temperatures stabilized as the tank burned off its contents. In Figure 34, it can be seen how half of the temperatures increase more rapidly since they are located above the liquid level and how the other half are only starting to increase after approximately 30 h.

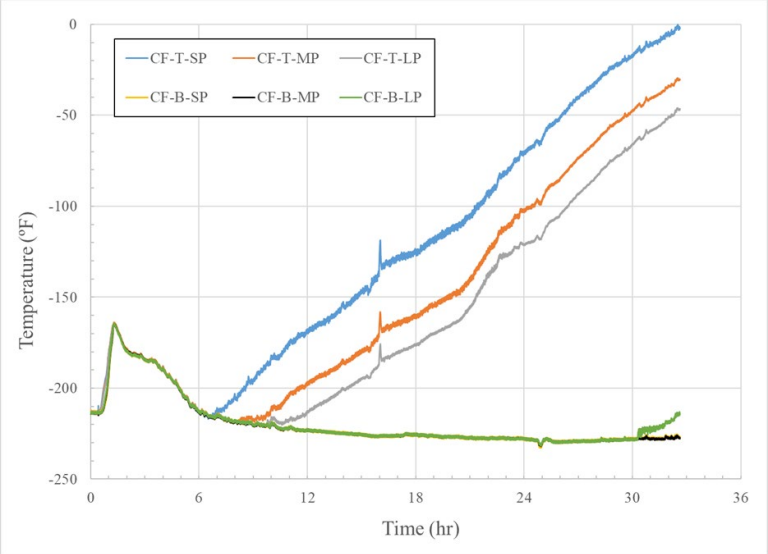


**Figure 32. Post-Test Internal Tank Temperature Data**

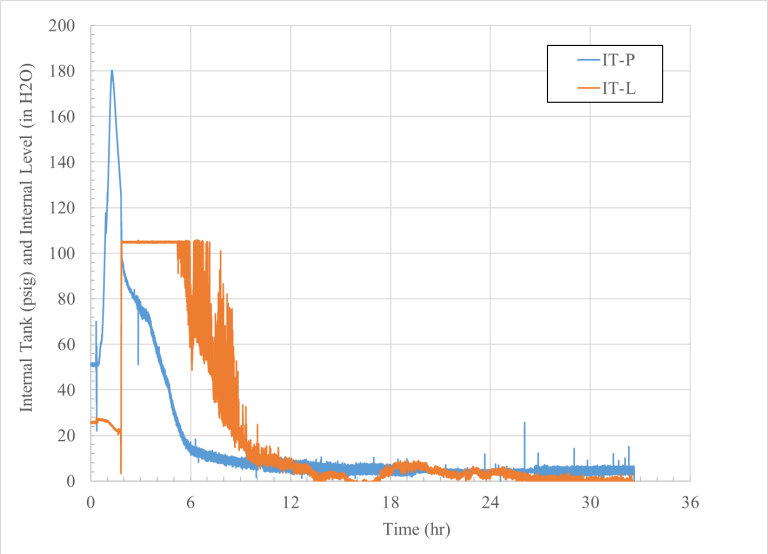


**Figure 33. Post-Test Internal Tank and Level Pressure Data**

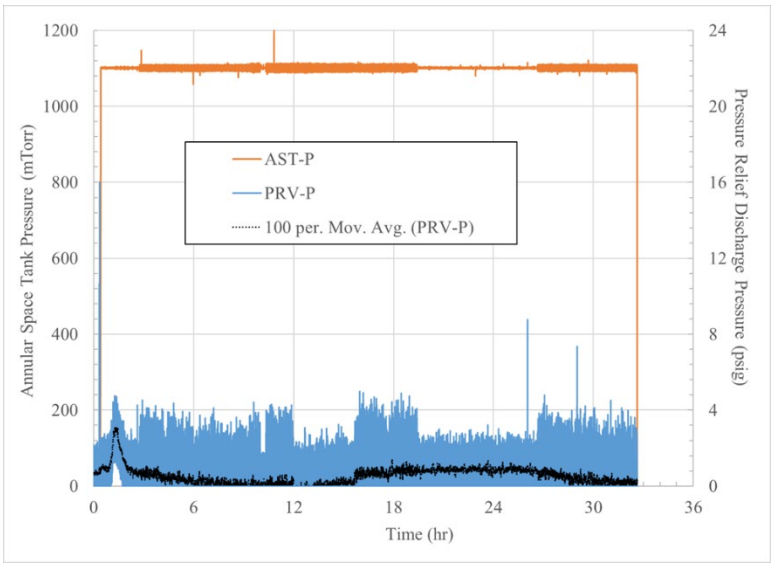


**Figure 34. Post-Test Annular Space and Pressure Relief Piping Pressure Data**

# 7. Data Analysis Results

This section provides detailed data analysis of the testing.

## 7.1 Initial Test Conditions

The initial conditions of the tests are provided in Table 6. The tank was filled around 4:30 pm on June 28, 2022. The fill volume was measured via a gauge on the filling truck. The fill level was checked using the analog liquid level gauge on the tank approximately 1 hour prior to the test (Figure 36). A liquid level sensor (Rosemount 2051C Coplanar Pressure Transmitter; Emerson) was used to estimate the volume of fluid throughout the test. The conversion of ΔP to a volume quantity requires the use of a formula which was provided in the form of a lookup table by Taylor Wharton. This lookup table assumes a liquid density of 423 kg/m$^3$.

The total mass of the lading transferred to the ISO container was calculated based on the measured volume of fill (i.e., 9500 gal) and the assumed density of the fluid at the time. The actual state of the fluid in the transfer truck was unknown, but discussions with Airgas indicates that it was expected to be at 111 K with a density of 423 kg/m$^3$. This equates to a total lading mass of 15,212 kg (33,537 lb).

The pressure sensor was positioned in a box in the ground approximately 3 m (10 ft) below the tank's standard pressure gauge (Figure 35). This equates to an increase in pressure (based on $P = \rho \cdot g \cdot h$) of 12,449 Pa (1.8 psi) from the tank's pressure gauge and the in-ground pressure sensor and corresponds with the ~2 psi difference between the two readings (see Table 6).

The quality of the two-phase mixture (0.00116), a ratio of the mass of vapor to the total mass of the mixture, was calculated for the state of the system at the time of fill using the assumptions and measurements detailed above.

**Table 6. Initial Conditions**

| | At filling | At t=0 |
|---|---|---|
| LNG Composition (% $CH_4$) | 99.6% | |
| LNG Volume (m$^3$ [gal]) [Truck gauge] | 35.96 [9500]* | - |
| LNG Volume (m$^3$ [gal]) [Tank gauge] | - | 33.02 [8,724]* |
| LNG Volume (m$^3$ [gal]) [LL Sensor] | - | 32.77 [8,657770]* |
| LNG Mass (kg [lb]) [LL Sensor] | - | 15,212 [33,537]* |
| Tank Pressure-absolute (kPa [psia] ) [Tank gauge] | - | 439 [63.7] |
| Tank Pressure-absolute (kPa [psia]) [Sensor] | 418,512 [60.7]** | 453 [65.7] |
| Tank Internal Temperature (K [F]) | 137 [-213]** | 136.7 [-213.6] |
| Quality of two-phase mixture | 0.00116 | 0.003631 |
| Annular Space Pressure (mTorr) | 33 | 28 |

- Not measured.
* This value is sensitive to variations in fluid density, temperature, and pressure (LL Table provided by Taylor Wharton assumes a density of 423 kg/m$^3$; 111 deg K; 97 kPa).
**The upper internal tank was still cooling when this measurement was taken.


**Figure 35. Pressure Gauge on Tank Indicating ~49 psig (337,843 Pa gage) 1 h Prior to Test**


**Figure 36. Liquid-level Gauge on Tank Indicating ~25.9" $H_2O$ 1 H Prior to Test**

The fluid properties at t=0 were estimated based on the measured data provided in Table 6 with the assumption that the fluid was at steady state and fully saturated. These data are summarized in Table 7.

**Table 7. Fluid Properties at t=0 (Saturated Properties) [Data from NIST Chemistry WebBook Standard Reference Database (SRD) Number 69]**

| Property | Liquid | Gas/Vapor |
|---|---|---|
| Temperature (K) | 136.7 | 145.7 |
| Pressure (MPa) – absolute | 0.53835 | 0.85139 |
| Density (kg/m$^3$) | 382.7 | 13.381 |
| $C_p$ | 3.7551 | 2.7626 |
| $C_v$ | 1.9558 | 1.7470 |
| Sound Speed (m/s) | 1074.7 | 286.3 |

Figure 37 shows that the average start-of-test temperature recorded by the 11 TCs submerged in the fluid was 136.7 K (minimum = 135.6 K, maximum = 137.7 K). For the seven TCs exposed to the vapor space but attached to a float, the average start-of-test temperature was 136.7 K (minimum = 136.0 K, maximum = 137.5 K). For the six TCs exposed to the vapor space but attached to the internal tank, the average start-of-test temperature was 145.7 K (minimum = 144.5 K, maximum = 147.2 K). The difference in the vapor temperatures is most likely due to the different mounting surfaces used (i.e., floats vs tab welded to internal tank wall). Figure 38 shows closeup views of each type of TC mounting.

The float-mounted vapor-space TCs were designed to sit 6.5 to 14 in. above the surface of the liquid. At the start of the test the tank-mounted vapor-space thermocouples were located 50-127 mm (2-5 in.) above the surface of the liquid (at 74-78 percent fill).

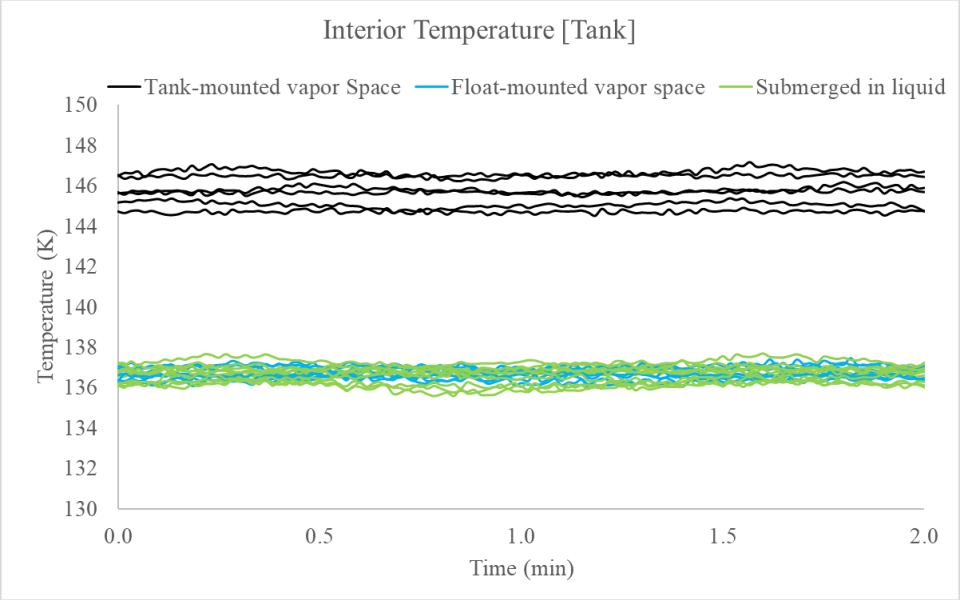


**Figure 37. Steady-state Internal Temperature Prior to Test**


**Figure 38. Vapor-space TCs; Tank-mounted (left), Float-mounted (right)**

## 7.2 External Heating

Incident heat flux to the external tank was measured via six DFTs evenly spaced along the approximate centerline of the tank (three on each side) and three DFTs under the railcar.

The data from these DFTs (Figure 39), supplemented by Fire Dynamics Simulator (FDS) models, were used to predict the total heat load to the external tank during the fire test and calibrate an FDS model. The resulting FDS data (i.e., incident heat flux) was used to create a higher resolution map of heat flux onto the tank that was summed over the total external area of the tank.

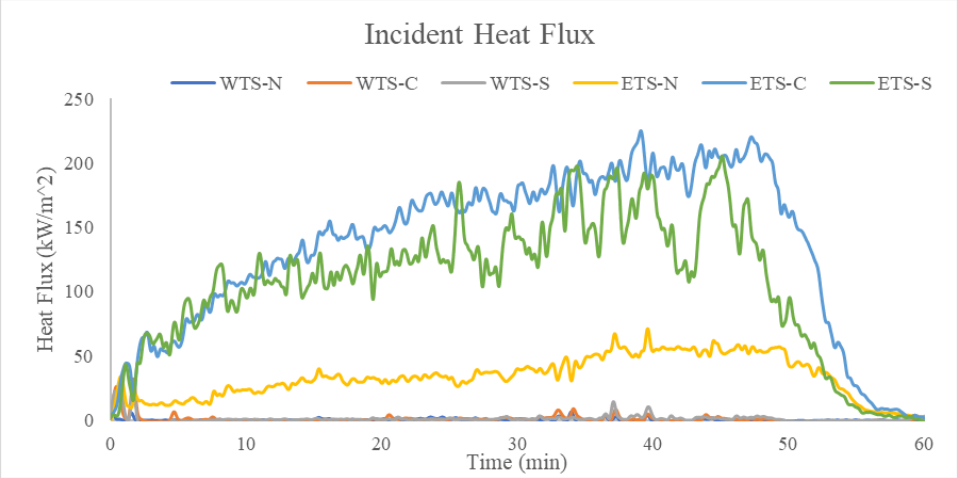


**Figure 39. Incident Heat Flux to External Tank During Fire Test**

Heating was asymmetrical due to wind activity with the East side of the tank subjected to much greater heat flux than the West side of the tank.

Based on the data and FDS simulations the total incident heat applied to the external tank progressively increased throughout the test and was calculated to peak at 3900 kW at 37.2 min and at 3885 kW at 44.7 min as shown in Figure 40.

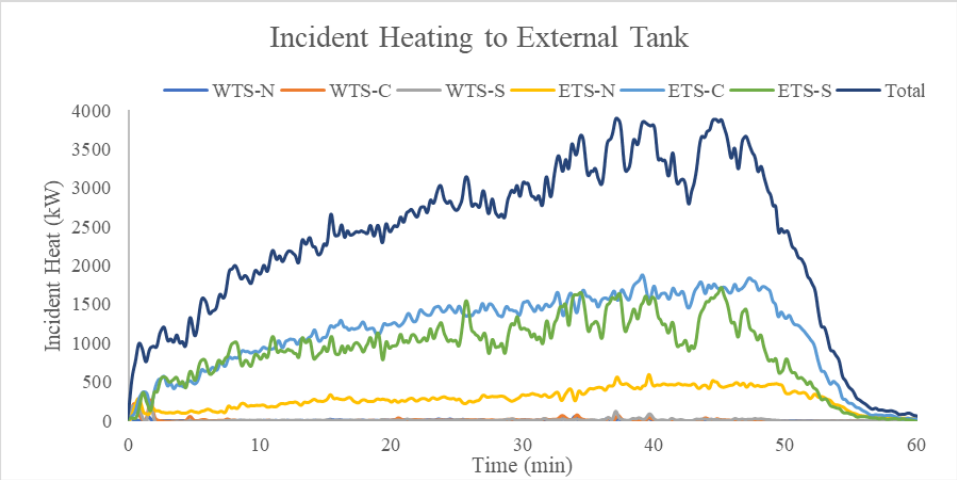


**Figure 40. Incident Heating to External Tank During Fire Test**

The average incident heat during the last 10 minutes of active propane flow (t=38 min to t=48 min) was 3497 kW, while the average heating for the proceeding 10 min was 10 percent lower at 3129 kW. The cumulative heat applied to the tank (Figure 41) was calculated to be 7.35 GJ during the 48 min of full propane flow and 8.29 GJ during the 56 min of the fire test.

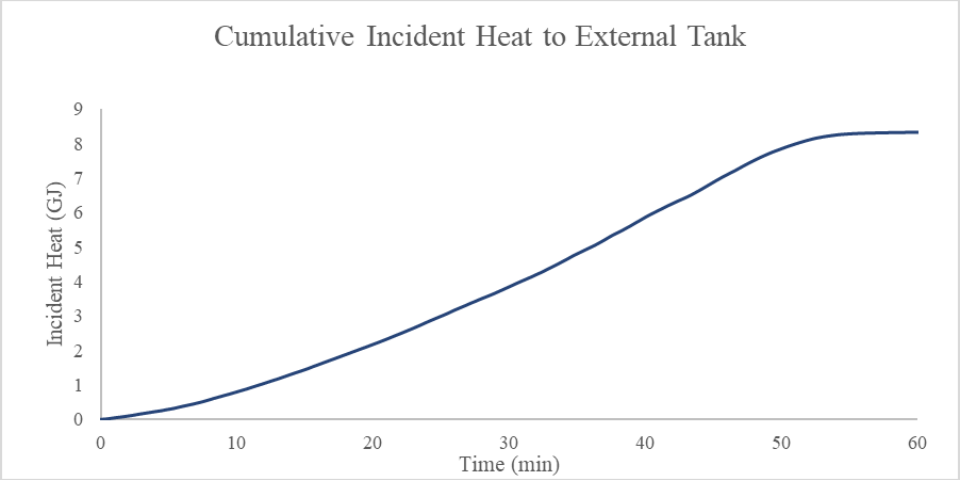


**Figure 41. Cumulative Incident Heating to External Tank During Fire Test**

## 7.3 Internal Temperature

The internal tank temperatures were recorded with numerous TCs located within the nominal liquid and vapor space. The data recorded by these sensors are provided in Figure 42 through Figure 46.

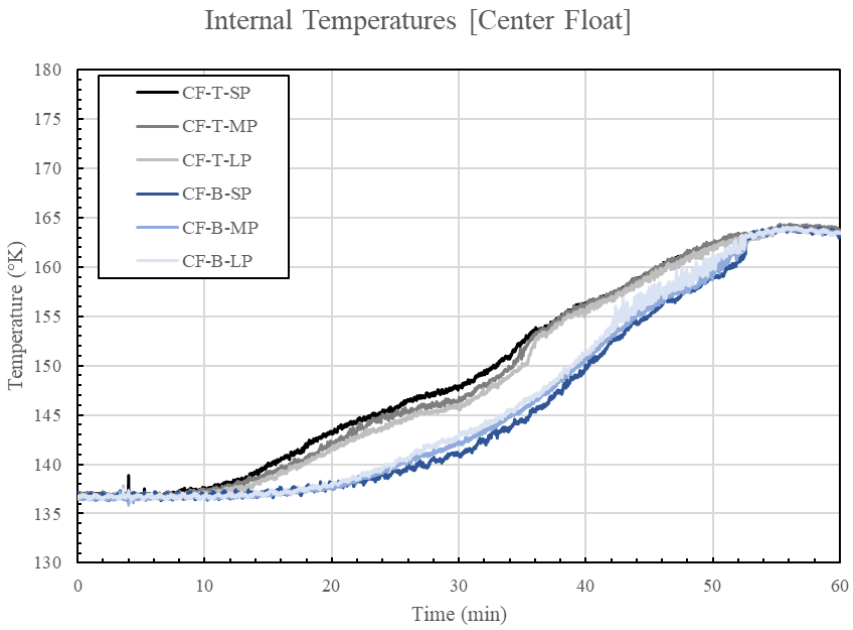


**Figure 42. Center Float Thermocouples: "T" Denotes Gas Phase Region & "B" Denotes Liquid Phase Region**

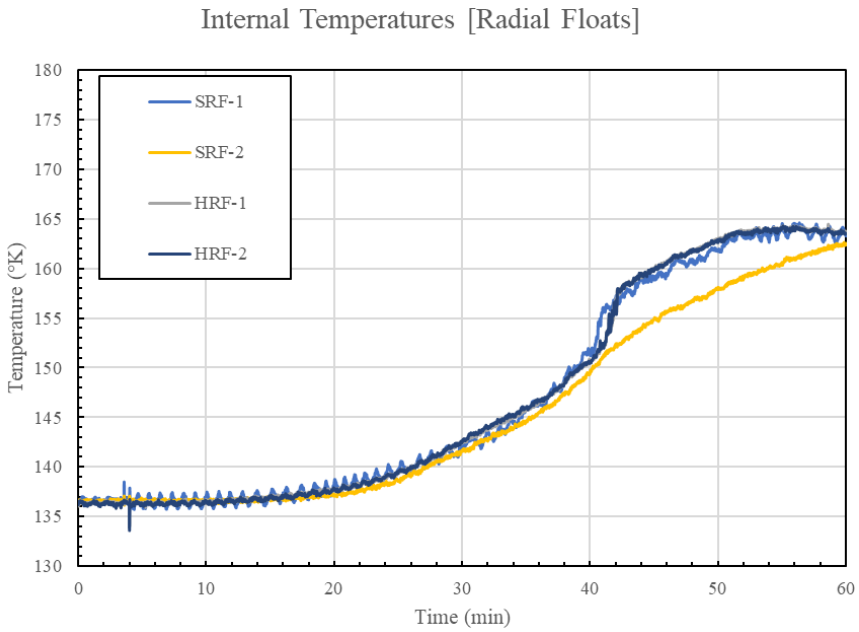


**Figure 43. Radial Float Thermocouples: "SRF" Denotes Shell Radius & "HRF" Denotes Head Radius**

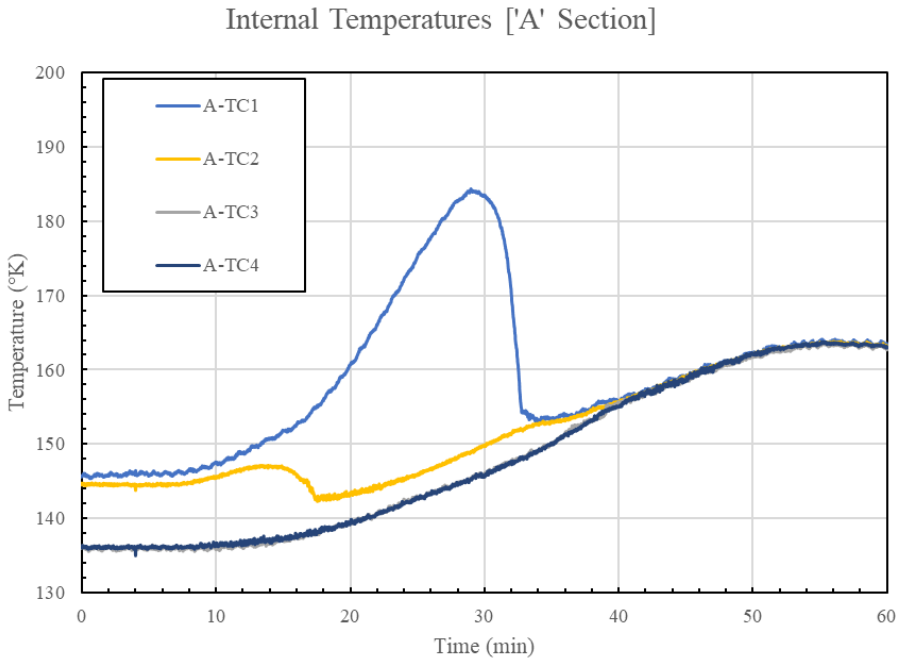


**Figure 44. Thermocouples in the "A" Section**

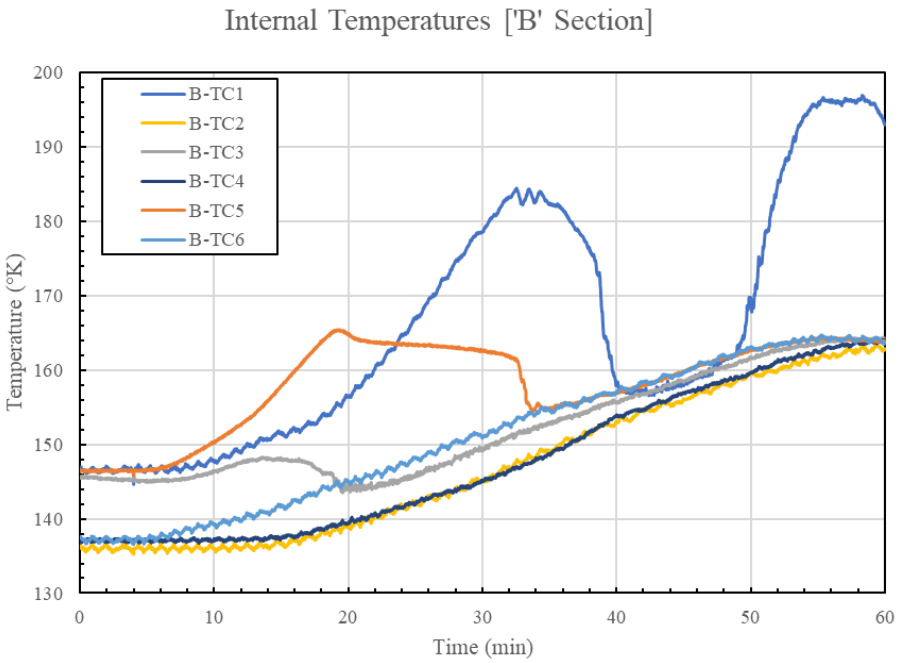


**Figure 45. Thermocouples in the "B" Section**

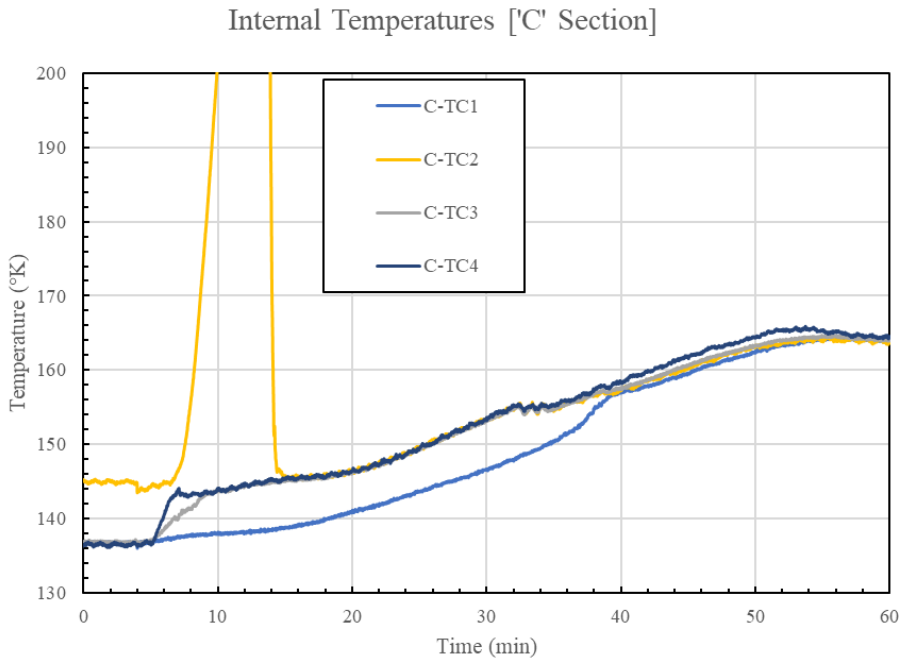


**Figure 46. Thermocouples in the "C" Section**

The total change in temperature over the duration of the fire test was approximately 29 deg K with a maximum liquid temperature of 165.7 K. The temperature began to rise roughly 8 min into the fire test. The vapor space temperature, as indicated by the center float, increased more rapidly than the liquid from t=12 min through to propane shutoff at which point the temperatures converged.

Some anomalies in the recordings are apparent in the data, possibly due to exposure of the TC wires to the extreme heat. In aggregate, the temperature data demonstrated a consistent temperature rise throughout the test.

The rate of temperature change of the LNG increased throughout the test until it peaked at 1.7 deg K per minute at t=42.8 min, roughly the same time the tank heat flux peaked (Figure 47). After peaking, the rate of temperature change decreased, trending to zero at roughly t=58 min.

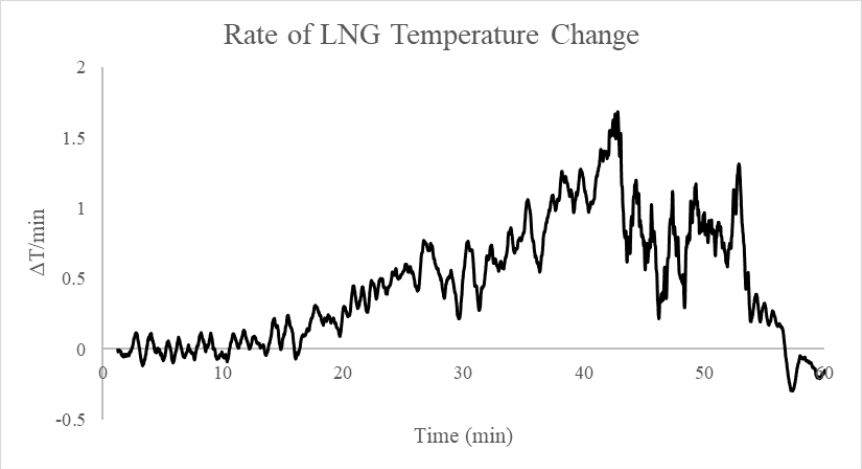


**Figure 47. Rate of LNG Temperature Change**

## 7.4 Internal Pressure

The internal tank pressure rose steadily after burner ignition and continued to rise until the burner was extinguished (Figure 48). The maximum pressure reached during the test was 1.24 MPa (180.3 psig) at t=55 min. Three PRD activation events occurred during the fire portion of the test at 00:32:20, 00:33:19, and 00:34:03 and can be clearly seen in the time history curve in Figure 48.

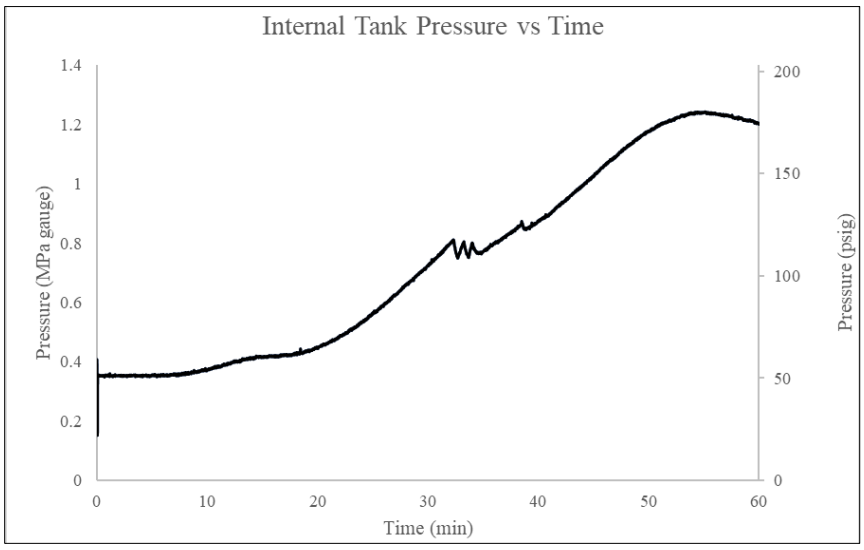


**Figure 48. Internal Tank Pressure vs Time for the First 60 Minutes of the Test**

Figure 49 shows the rate of change of the internal tank pressure.The pressure began to increase approximately 7 min into the test at an average rate of 2 psi/min. The maximum rate of pressure increase (5.6 psi/min) occurred just prior to initial PRD activation (~00:32:20). Rapid decreases in pressure (-10 to -25 psi/min) occurred simultaneously with each of the three PRD activations. After re-seating, rapid increases in pressure (15 to 20 psi/min) occurred briefly before returning to nominal rates (~3.6 psi/min). The rapid but un-sustained rate of pressure loss during the initial 15-20 s of PRD activation is possibly related to inertial effects of the fluid within the pressure sensor tube moving due to the transient opening event.

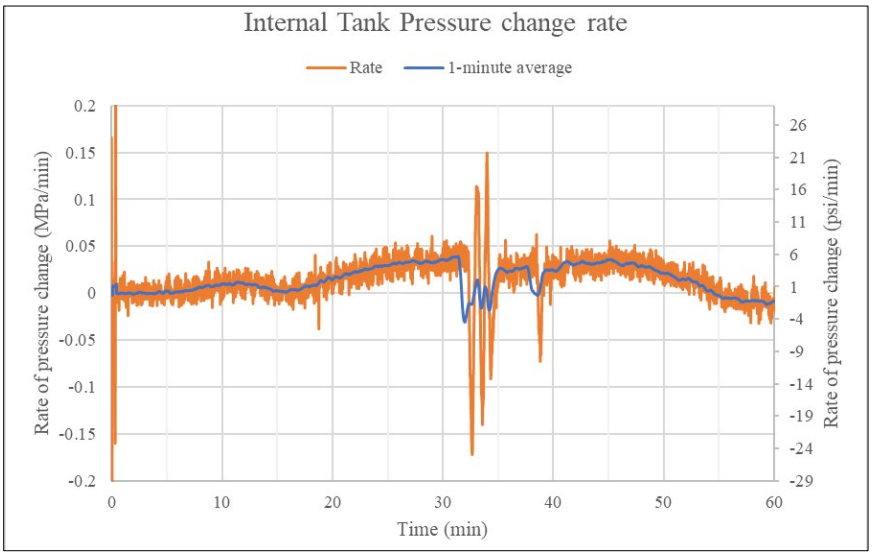


**Figure 49. Rate of Change of Internal Tank Pressure**

During periods of continuous PRD activation with maximum fire engulfment (00:34:03 – 00:48:16), the rate of pressure change varied from 3.2 psi/min to a maximum of 5.2 psi/min with an average rate of 3.6 psi/min. The maximum rate of internal tank pressure changes over this period (5.2 psi/min) occurred 3 min prior to propane supply shutoff (00:45:20). Just prior to propane shutoff the pressure in the internal tank was increasing at a rate of 4.6 psi/min.

A rapid decrease in pressure from 00:38:30-00:38:45 (~15 second duration) occurred at the same time and for the same duration that the PRD jet flame was observed to significantly increase in size (Figure 50). The cause of this response is unknown but may be due to the opening and re-closing of the second PRV.

**Figure 50. PRV Flame Comparison Prior to (left) and During (right) the Rapid Pressure Drop [~00:38:30]**

A substantial pressure drop was noticeable approximately 87 min into the test (Figure 51). This occurred shortly after the piping end cabinet became fully engulfed in flames following the failure of the aluminum service panel (Figure 52).

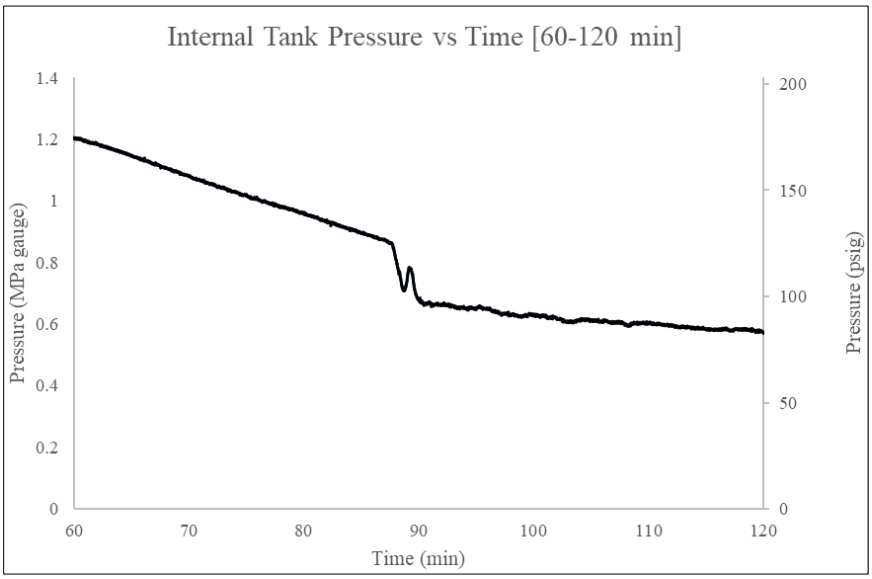


**Figure 51. Internal Tank Pressure vs Time [60-120 min]**

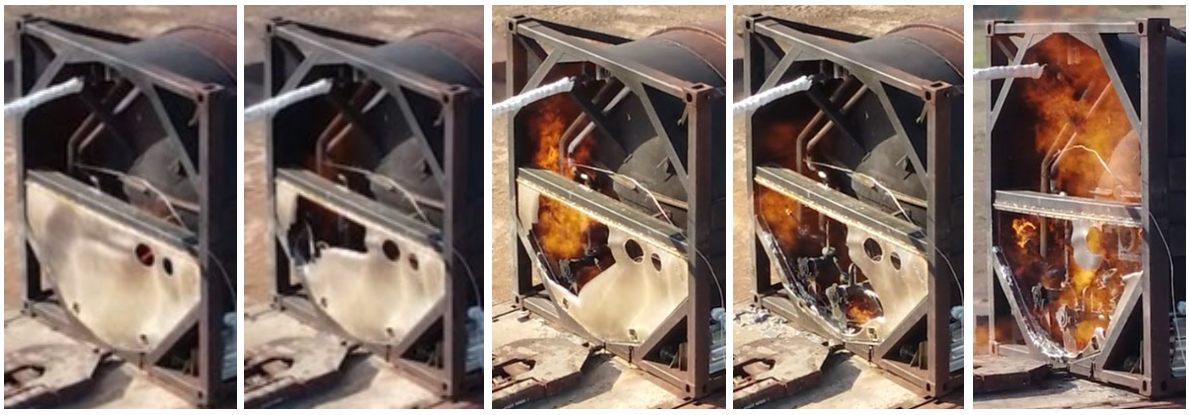

**Figure 52. Progression of Piping Cabinet Door Failure over ~3 Min 50 s; Note the Increase in Fire Size as More of the Door is Melted [1:21:47 – 1:25:37]**

It is likely that the packing material within the globe, ball, and needle valves in that area suffered thermal failures and allowed natural gas to leak out and catch fire. These valves and their maximum working temperatures are summarized in Table 8 for reference. The drop in pressure is most likely due to the increase in gas leakage out of the tank through the failed service valves.

**Table 8. General Summary of Installed Valves and their Working Temperature**

| Description | Maximum working temperature (C [F]) |
|---|---|
| Herose, ½”-2” Globe, SS Body, Bronze Top Work | 120 [248] |
| Fire Block, 1”-2”, Ball, SS | 180-200 [356-395] |
| Generant, ½”, High Pressure Relief Valve | 121-232 [250-450] |
| Hy-Lok, ¼” Needle, SV-NV, SS | 315 [600] |

For the remainder of the post-test events, the tank pressure continued to decrease without any substantial rate change or noticeable events (see Figure 53 and Figure 54).

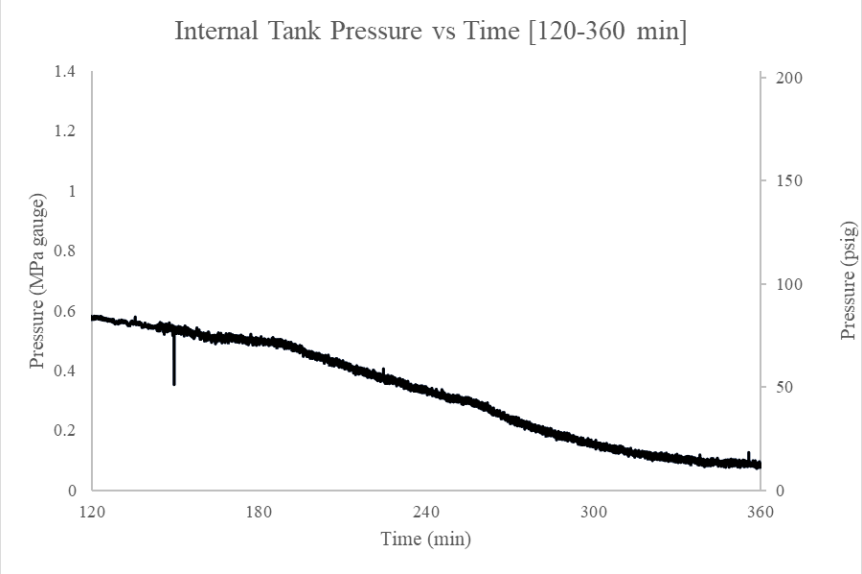


**Figure 53. Internal Tank Pressure vs Time [120-360 min]**

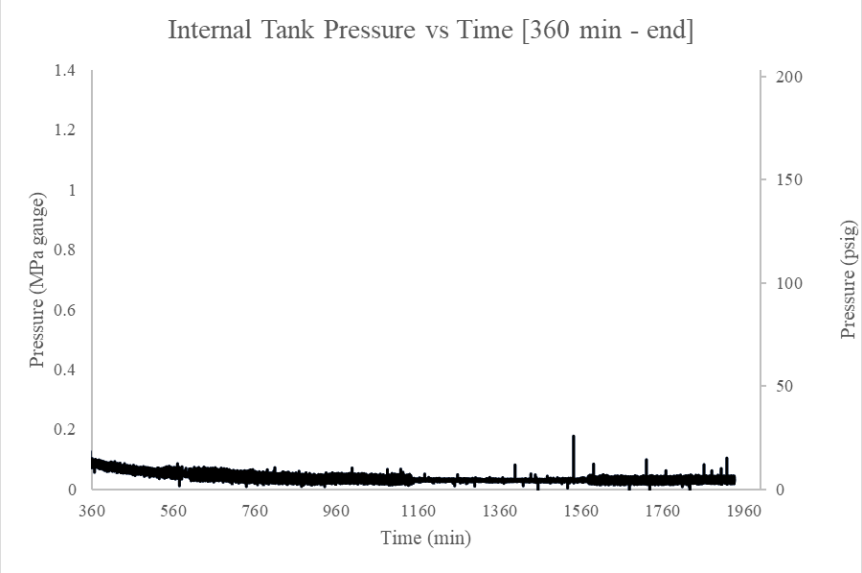


**Figure 54. Internal Tank Pressure vs Time [360 min- end]**

## 7.5 PRV Response

PRV actuation was confirmed through video (i.e., static and drone cameras) in combination with audio captured in the video recordings and supported by simultaneous transient pressure readings. The PRV pressure sensor, which was mounted in the exhaust pipe downstream of the PRVs, did not produce any usable data. The response appeared very different from that collected in the previous test with LN2.

The PRV system activated three separate times during the fire portion of the test. The PRV exhaust was ignited within approximately 1 s of opening each time. Each opening event can be

seen in the pressure vs time plot in Figure 48. It is unknown whether one or both valves were open during these activation events.

The PRV system actively released fluid into the atmosphere for 1374 s (22 min and 54 s) during the fire portion of the test. The PRV system continued releasing fluid from the PRV for the duration (6 h) of the video footage.

The size of the PRV exhaust cloud and flame decreased significantly, but did not stop, after 90 min. This is coincident with the internal tank pressure dropping below the required PRV closing pressure (102.6 psig). One or both PRVs were most likely thermally damaged and unable to fully seal by this point even though the internal pressure had dropped below their designed closing pressure. The PRV exhaust and piping cabinet valve leaks continued to burn for the duration of the video (6 h) with behavior like that shown in Figure 55.

**Figure 55. Typical Post-Test Piping Cabinet Fire Behavior [04:23:33]**

## 7.6 Mass Loss and Fluid Heating

The total mass lost during the test was estimated based on calculated nominal PRV pressure-dependent flow rates. The flow rates are provided by the manufacturer for air but were calculated specifically for methane using the orifice equation method.

The estimated mass loss for the fire-portion and post-fire periods of the test are summarized in Table 9. The cumulative mass loss versus time for the fire-portion of the test is provided in Figure 56.

**Table 9. Estimated Mass Loss**

| Duration | Single PRV | Both PRVs |
|---|---|---|
| 22 min 54 s (fire-portion; up to burner extinguish) | 684 kg (1508 lb) | 1368 kg (3016 lb) |
| ~36-48 h (post-fire; remaining fluid) | 13078 kg (28832 lb) | 12394 kg (27324 lb) |

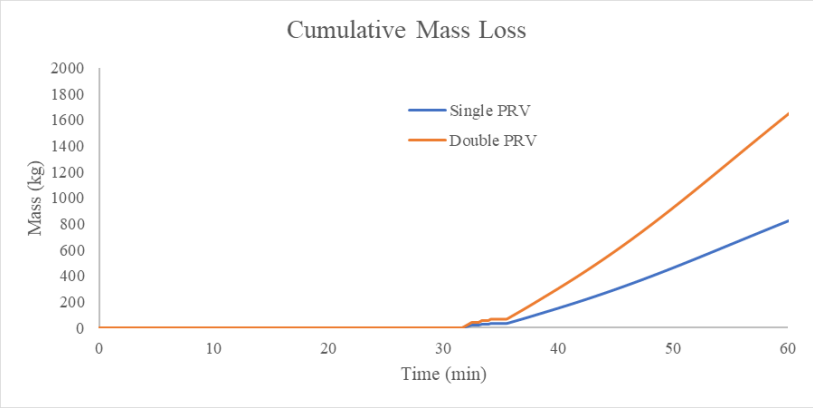


**Figure 56. Cumulative Mass Loss vs. Time**

The amount of heat absorbed by the fluid during the fire test can be estimated by summing the energy required to 1) increase the temperature of the fluid (liquid and vapor) during the test (i.e., Sensible heat), and 2) vaporize enough liquid to account for the mass of vapor exhausted from the PRV system (i.e., Latent heat). High and low estimates of heating requirements were calculated based on whether a single PRV or both PRVs were active. The relief valve calculation code (CGA S-1.2-2009, Section 5.3) assumes that PRV performance is additive (i.e., the exhaust capacity for 2 PRVs is twice the capacity for 1 PRV). However, the response of multiple PRVs is likely to be dependent on their actual installation.

Table 9 shows a summary of the heat input to fluid during the fire test. The amount of heat energy required to raise the temperature of the fluid during the test was calculated using the temperature-dependent heat capacities of methane (liquid and vapor) along with the time-dependent remaining fluid mass and time-dependent temperature change. The incremental heat required was calculated at 1 s intervals. The fluid was assumed to heat evenly due to convective mixing.

**Table 10. Summary of Heat Input to Fluid during 56 Min Fire Test**

| | Single PRV | Double PRV |
|---|---|---|
| Sensible heat (GJ) | 0.693 | 1.386 |
| Latent heat – Exhaust (GJ) | 0.261 | 0.522 |
| Total heat (GJ) | 0.954 | 1.908 |

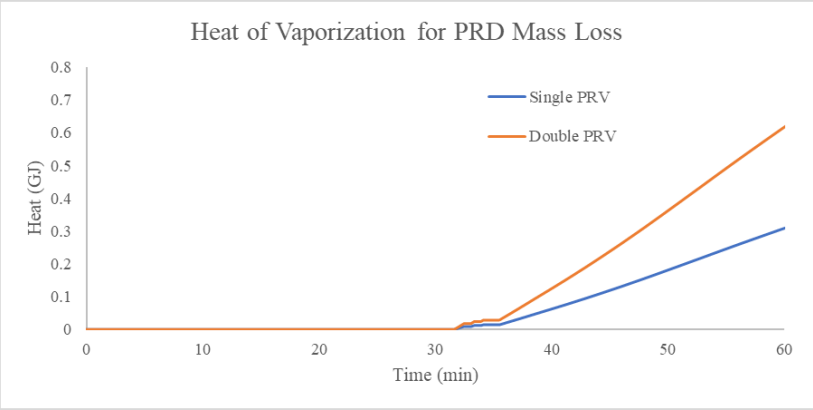


**Figure 57. Heat Required to Vaporize Fluid to Account for the Vapor Exhausted from the PRV System**

As the bulk fluid was heated throughout the test, the saturated liquid density decreased, causing it to take up more volume. The increase in liquid volume during the test can be seen in Figure 58. Depending on the amount of mass exhausted from the system (one or two PRV flow), the relative mass of liquid may increase or decrease (Figure 59).

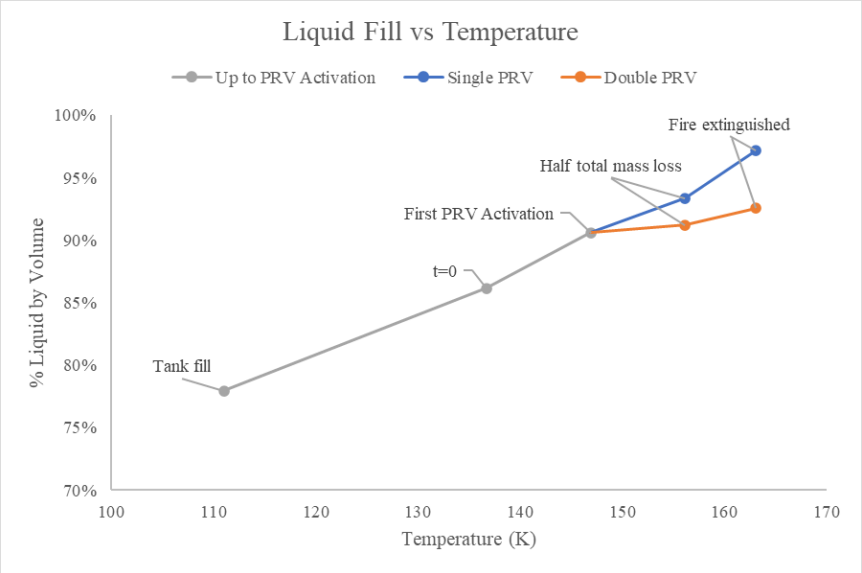


**Figure 58. Percent Liquid (by Volume) vs. Bulk Fluid Temperature at 7 Key Data Points**

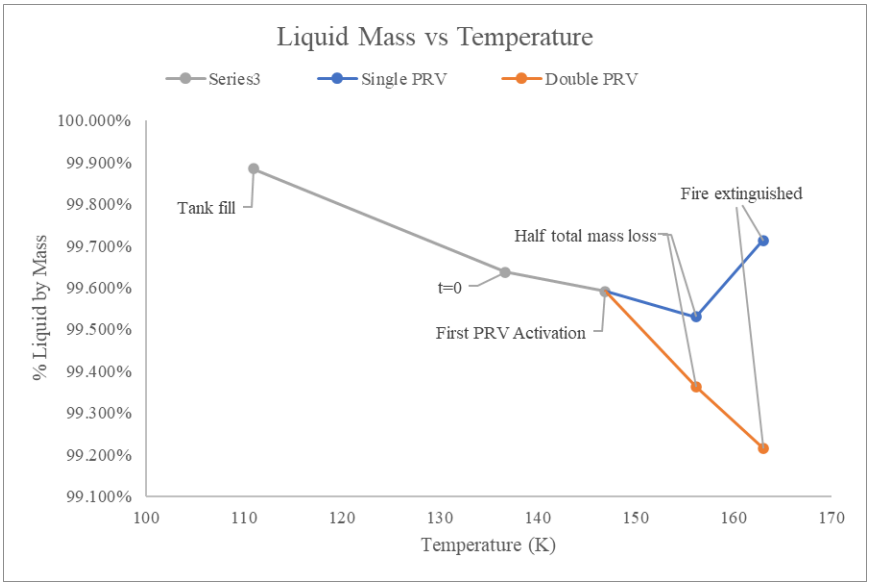


**Figure 59. Percent Liquid (by Mass) vs. Bulk Fluid Temperature at 7 Key Data Points**

As heat was added to the closed system (up to first PRV activation) the mixture quality increased as the vapor density rapidly rose (Figure 60). Assuming single PRV flow, the mixture quality changed little during the ~23 min of PRV activation. Assuming double PRV flow, the mixture quality increased rapidly, indicating that the mixture was moving away from Saturated Liquid conditions.

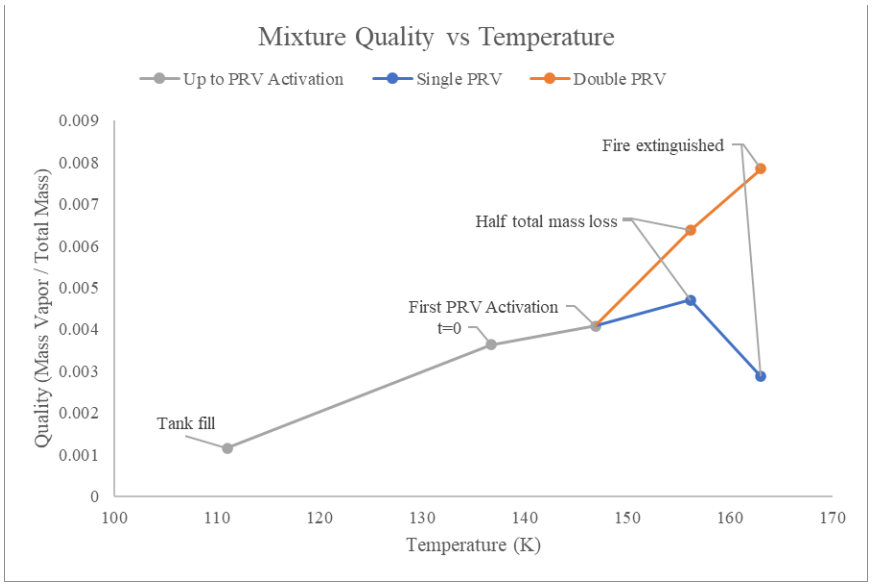


**Figure 60. Mixture Quality vs. Temperature at 7 Key Data Points**

Five key data points for the bulk fluid condition are plotted on the Pressure-Volume and Temperature-Volume curves for methane in Figure 61 and Figure 62. All points lie within the Vapor-Dome which confirms the presence of a two-phase mixture consisting of mostly Saturated Liquid.

The specific volume of the mixture remains constant in a closed volume (prior to PRV activation) with heating while pressure and temperature increase. After PRV activation, the pressure and temperature continued to increase along with increases in the specific volume of the mixture. This is consistent with a decrease in the percent liquid (by mass) of the system.

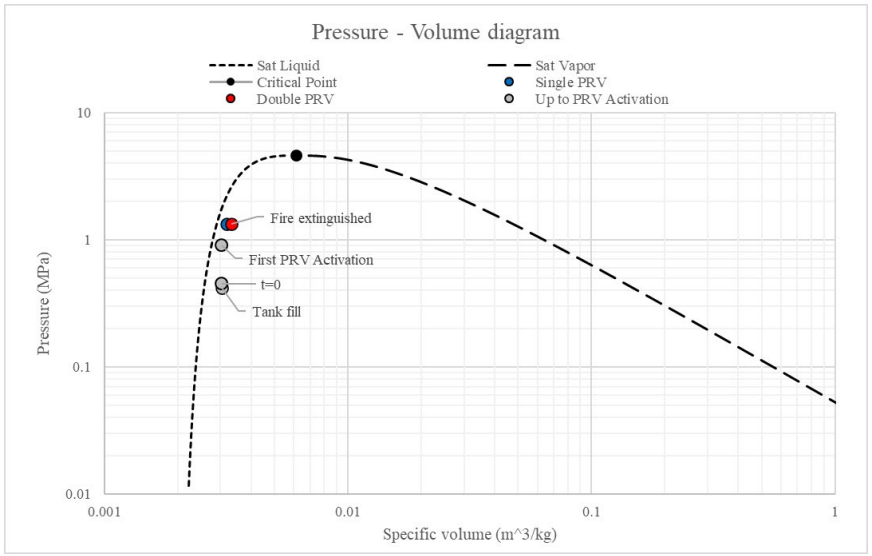


**Figure 61. Pressure vs. Specific Volume for 5 Key Data Points [Methane; NIST]**

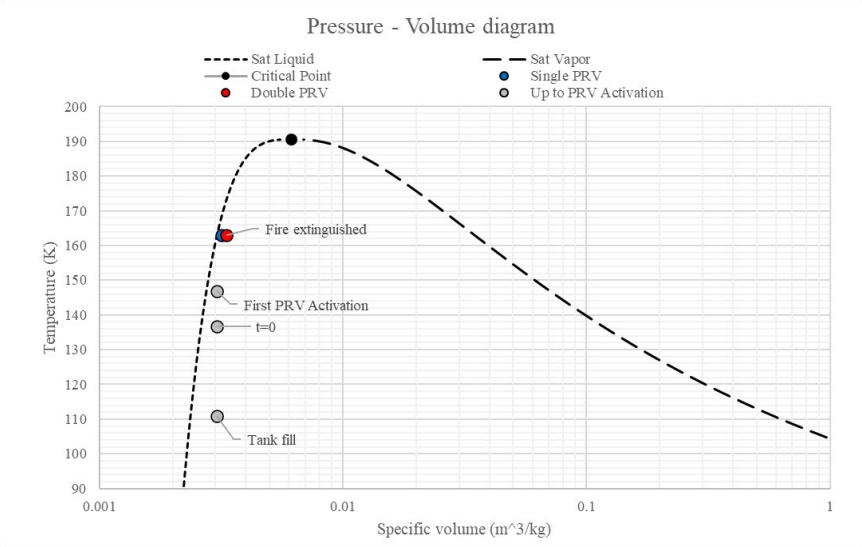


**Figure 62. Temperature vs. Specific Volume for 5 Key Data Points [Methane; NIST]**

## 7.7 PRV Jet Flame Response

The PRV exhaust ignited within 1 s of the valve opening. A mesh screen was positioned approximately 2 meters downstream of the exhaust to mitigate the chance of flashback. The screen also improved visualization of the flame and provided some obstruction to its motion. The "northwest" views in Figure 63, Figure 64, Figure 65, and Figure 66 show the difference in flame size based on the internal tank pressure. Greater tank pressure is clearly associated with greater PRV jet flame length in this scenario. Similar behavior can be observed from the drone-captured images in Figure 67, Figure 68, Figure 69.

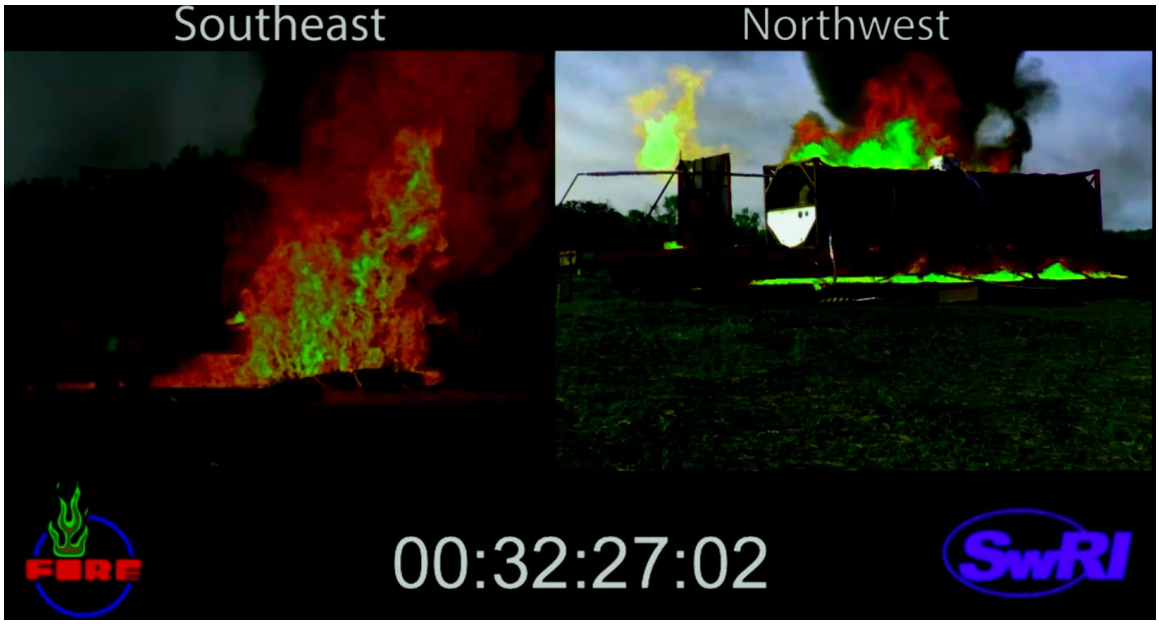


**Figure 63. Jet Flame Geometry at Internal Tank Pressure of 114 psi (PRD setting)**

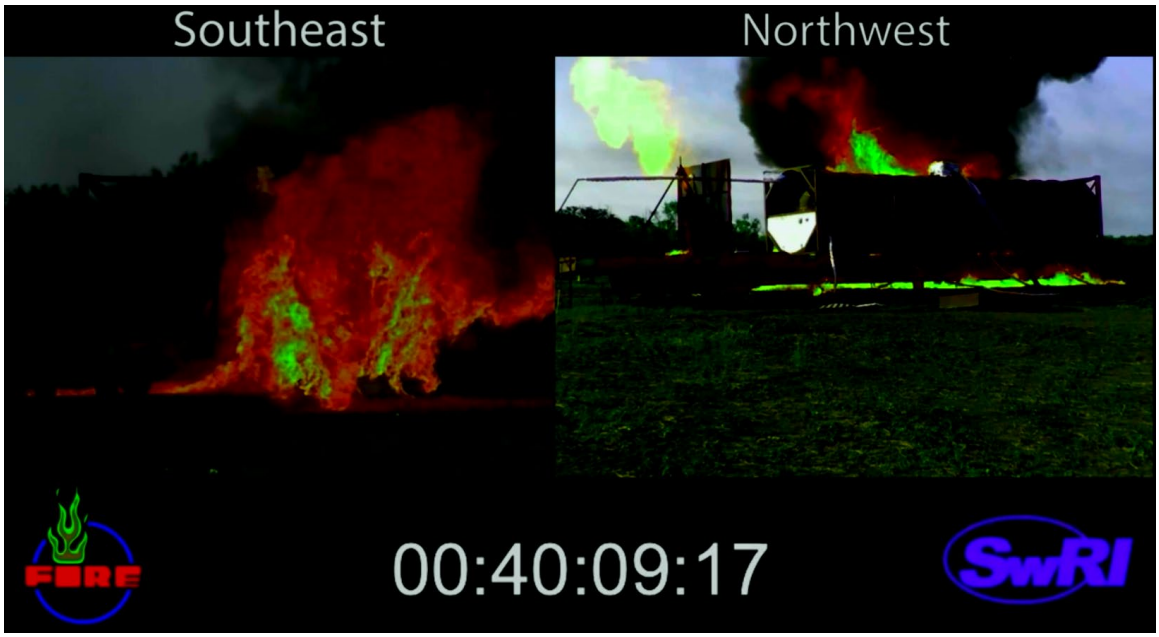


**Figure 64. Jet Flame Geometry at Internal Tank Pressure of 125 psig**

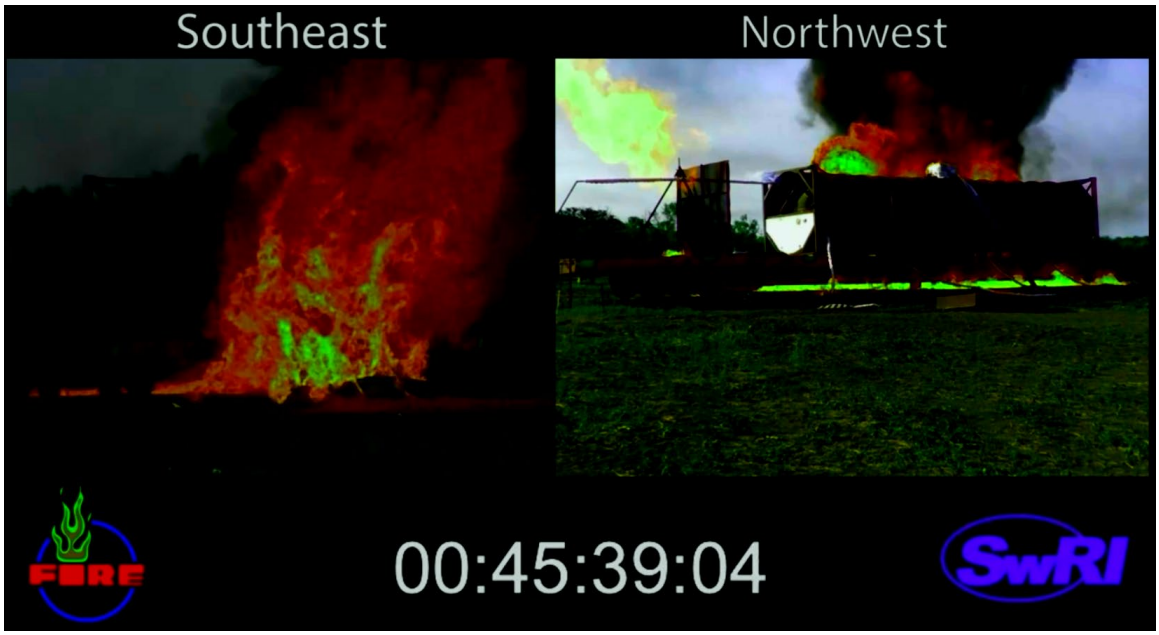


**Figure 65. Jet Flame Geometry at Internal Tank Pressure of 150 psig**


**Figure 66. Jet Flame Geometry at Maximum Internal Tank Pressure (180 psig); Note how Horizontal the Jet is with Most of the Flame Off-Screen to the Left**

**Figure 67. Jet Flame at Internal Tank Pressure of ~129 psig (view from drone) [~00:41:15]**

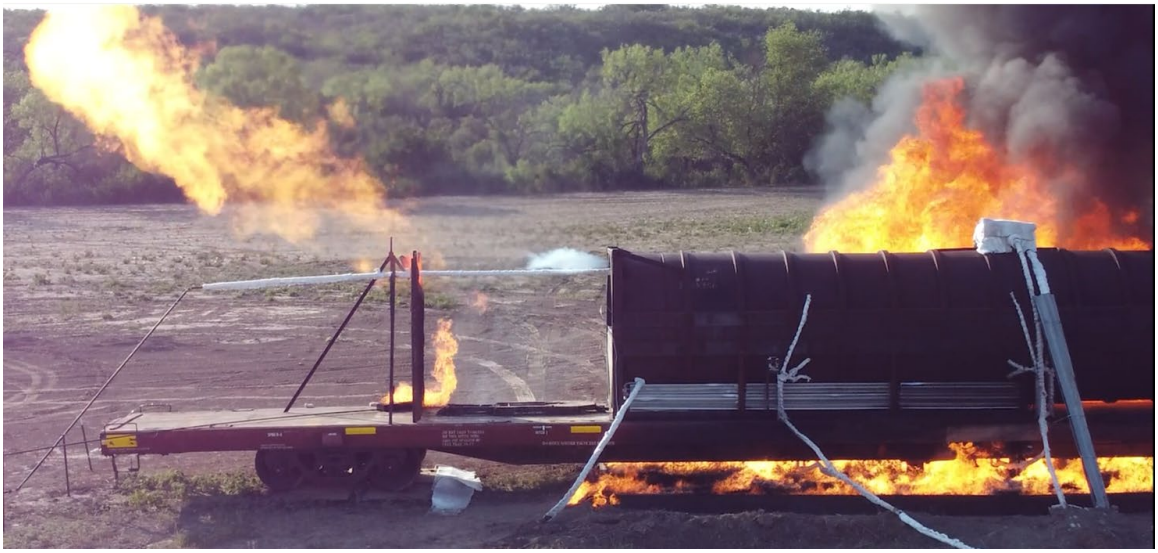

**Figure 68. Jet Flame at Internal Tank Pressure of ~156 psig [00:46:52]**

**Figure 69. Jet flame at Internal Tank Pressure of ~180 psig [00:56:00]**

**Figure 70. Frost on Deformed External Tank Jacket [1:07:24]**

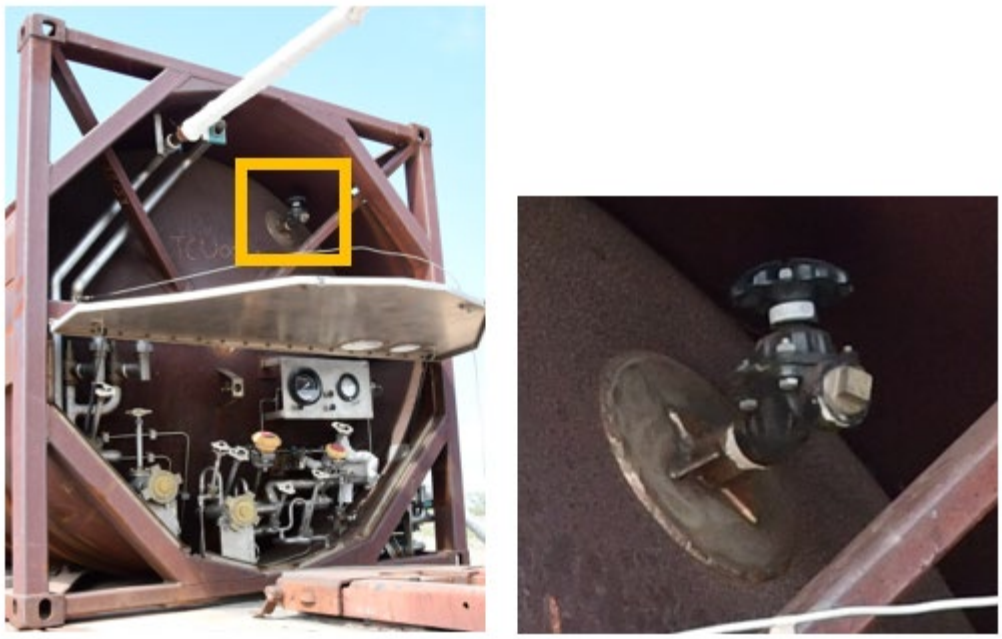

**Figure 71. Trycock Valve Prior to Test**

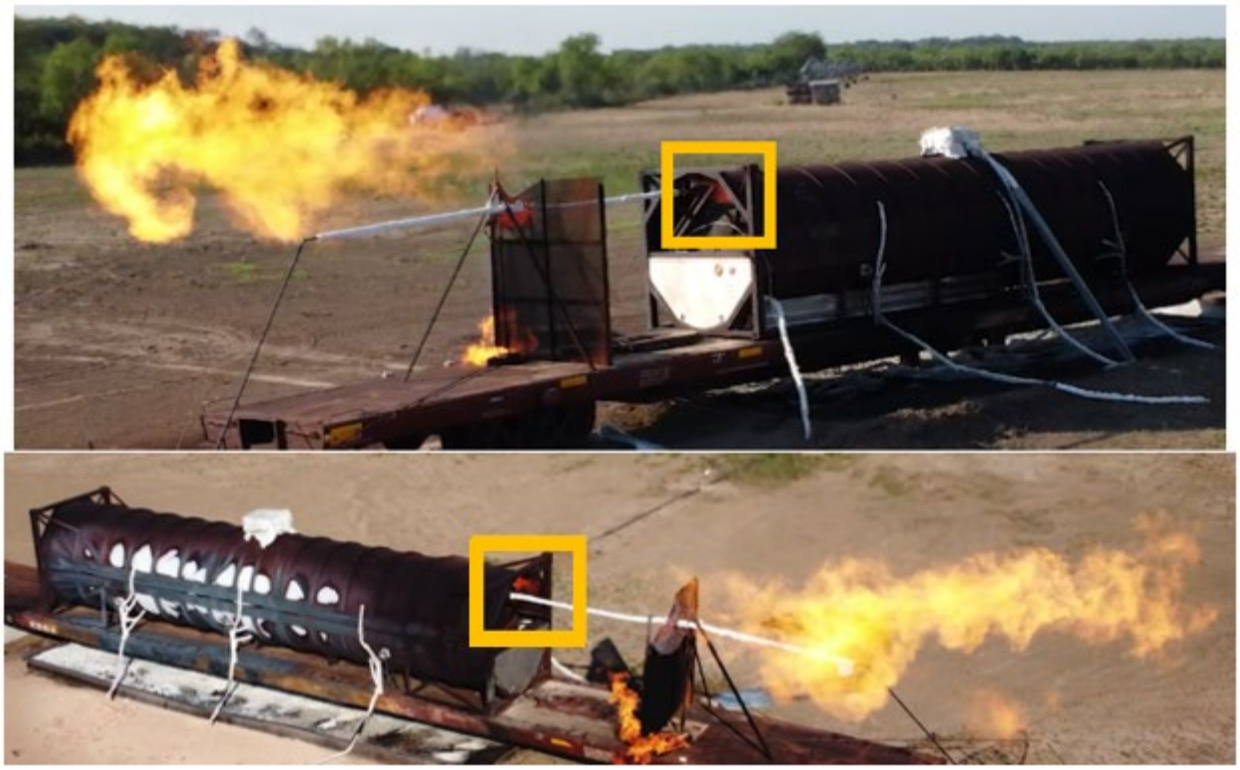

**Figure 72. Flames Observed at the Trycock Valve Location [~1:12:19]**

**Figure 73. View of Piping Cabinet Prior to (left) and Subsequent to (right) the Ignition of Leaked Gas [~1:12:20]**

# 8. Summary and Conclusions

In this Phase 2 research conducted in June of 2022, an ISO Tank filled with LNG was exposed to an LPG fire for approximately 56 min, after which the LNG continued to burn through the PRV and leakages in the piping cabinet for an additional 48 h. There was no BLEVE or other catastrophic failure observed during the test.

Based on the internal pressure rise and vacuum pressure measurement, the vacuum likely degraded relatively quickly into the fire exposure. The pressure inside the inner tank increased to a peak of approximately 180 psig. The PRV system worked properly, and the pressure valves began operating at approximately 114 psig. The valves intermittently reseated (at least partially) and reopened before fully opening for the majority of the test duration.

There was additional venting after the fire exposure stopped; this continued for more than two days. The pressure in the tank was at atmospheric level by the morning of July 1, 2022.

While one or more PRVs appeared to open at the specified set pressure and remain open for the duration of the test, the internal tank pressure and temperature continued to rise. While under full heat exposure from the pool fire the internal tank pressure rose at an average rate of 3.6 psi/min and up to 4.6 psi/min just before propane shutoff. If this trend were to continue the internal tank would reach 288 psi in another 30 min and 396 psi in another 60 min of fire exposure.

The pressure rise is, of course, related to the ability of the PRVs to remove mass from the internal tank. While the mass flow rates through the PRVs at elevated pressure in the configuration installed on the UN-T75 is not known, it is estimated that at the end of the fire test (180 psi) the flow through the PRV(s) was effectively choked. Thus, mass flow through the PRVs would not increase substantially with increasing tank pressure and the average pressure rise assumption is likely appropriate.

Future work could investigate the performance of the PRVs at elevated pressure and in their configurations as installed on the UN-T75.

## 9. References


1. Casal et al. (2001). Modeling and Understanding BLEVEs. Handbook of Hazardous Material Spills Technology, Chapter 22.

2. Casal, J. & Salla, J. M. (2006). Using liquid superheating energy for a quick estimation of overpressure in BLEVEs and similar explosions. *Journal of Hazardous Materials*.

3. Ke, W. (2009). CO2 BLEVE (Boiling Liquid Expanding Vapor Explosion). Masters Thesis.

4. Prugh, R. W. (1991). Quantify BLEVE Hazards. *Chemical Engineering Progress*.

5. Birk, A.M., Davison, C., & Cunnigham, M. (2007). Blast over-pressure from medium scale BLEVE tests. *J Loss Prev Process Ind, 20*, 194–206.

6. Genova, B., Silvestrini, M., & Trujillo, F.J. (2008). Evaluation of the blast wave overpressure and fragment initial velocity for a BLEVE event via empirical correlations derived by a simplified model of released energy. *J Loss Prev Process Ind, 21*, 110–117.

7. Baker, et. al. (2005). CPR 14E Yellow Book.

8. Raj, P. (2007). LNG fires: A review of experimental results, models and hazard prediction challenges. *Journal of Hazardous Materials, 140*, 444–464.

9. Huczek, J. (2016). Burning Duration Estimates.xlsx. Federal Railroad Administration.

10. Hurley, M., et.al. (2016). SFPE Handbook of Fire Protection Engineering, 5th Edition, Chapter 26: Heat Release Rates. Society of Fire Protection Engineers, 863-867.

11. Keltner, N., Nash, L., Beitel, J., Parker, A., Welsh, S., & Gilda, B. (2001). Fire Safety Test Furnace Characterization Unit. Thermal Measurements: The Foundation of Fire Standards, ASTM STP 1427. Dallas, TX. 128-146.

12. Beck, J. (1999). User's Manual for IHCP1D, a Program for Calculating Surface Heat Fluxes from Transient Temperatures Inside Solids. Beck Engineering Consultants Co., Okemos, MI.

13. ASTM E3057-16: Measuring Heat Flux Using Directional Flame Thermometers with Advanced Data Analysis Techniques. ASTM International, West Conshohocken, PA.

# Appendix A.
# CVA ISO Storage Tank Drawings

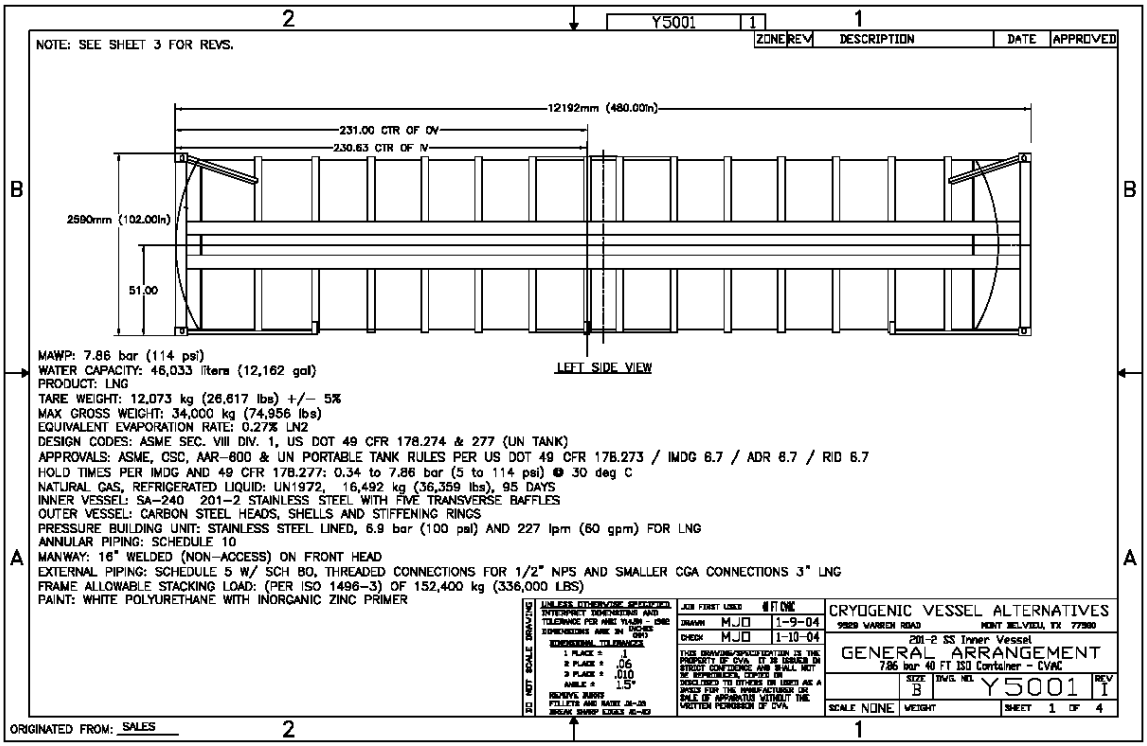


**Figure A-1. General Arrangement (Left Side) of CVA ISO Storage Tank**

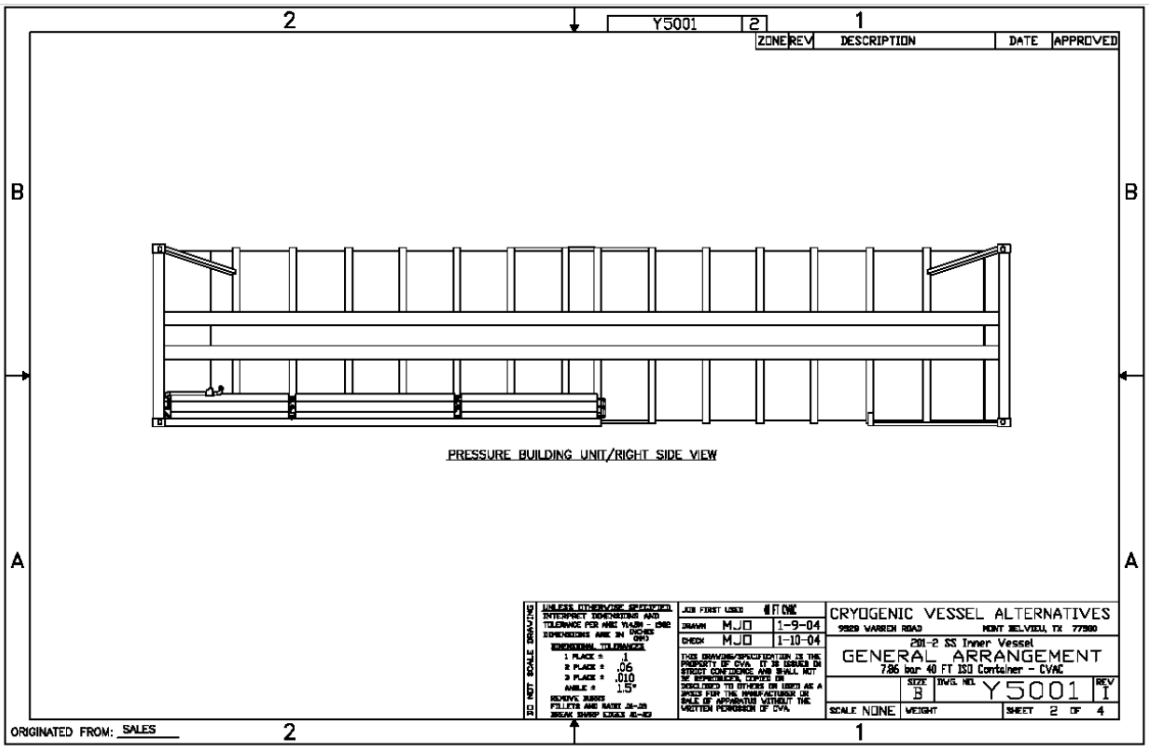


**Figure A-2. General Arrangement (Right Side) of CVA ISO Storage Tank**

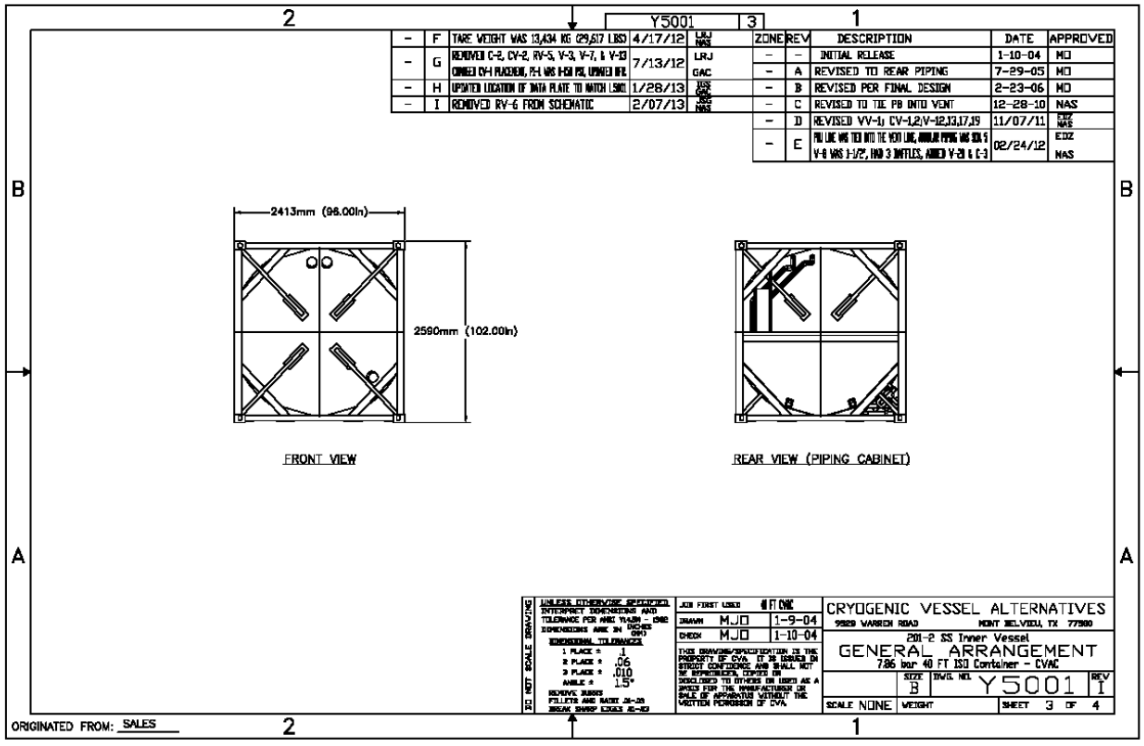


**Figure A-3. General Arrangement (Front and Rear Sides) of CVA ISO Storage Tank**

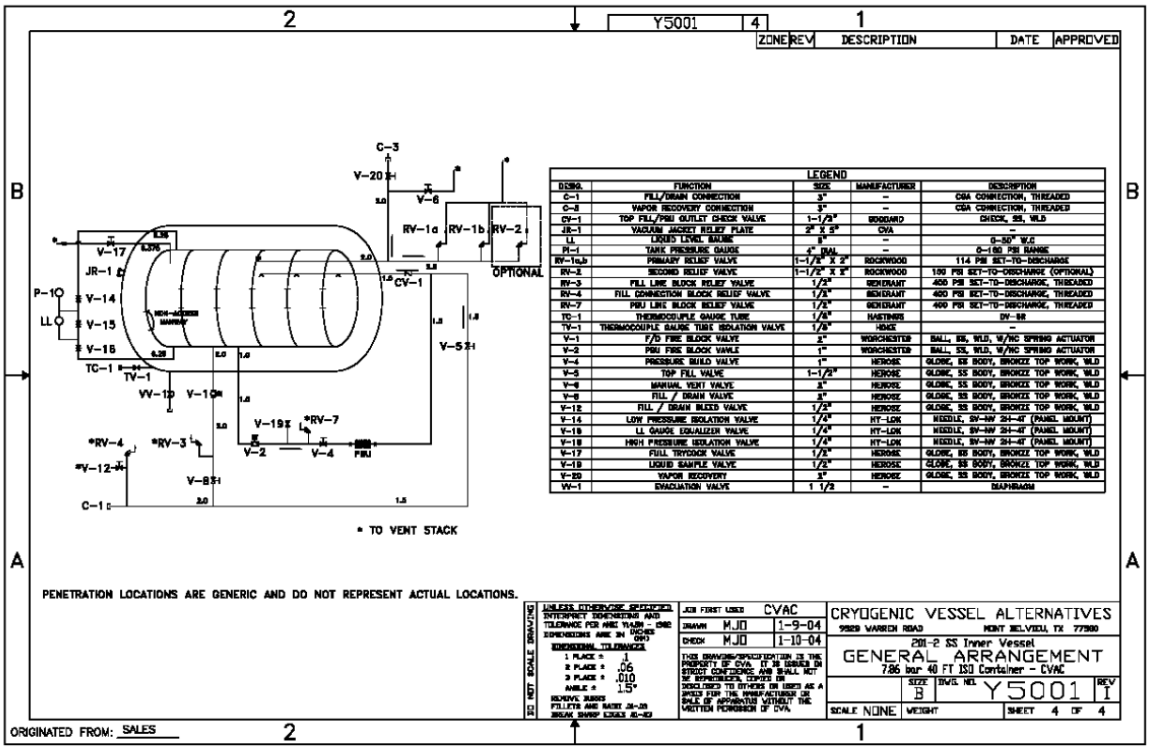


**Figure A-4. Piping Arrangement of CVA ISO Storage Tank**

# Appendix B.
# Instrumentation Drawings

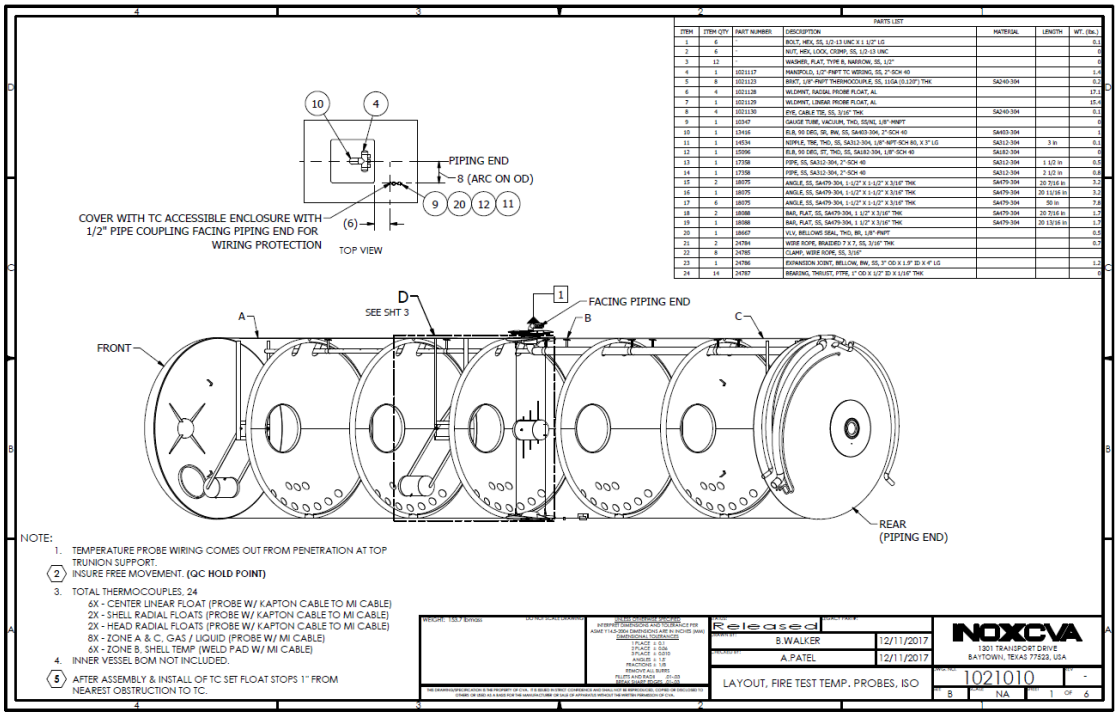


**Figure B-1. Overall Arrangement of Thermocouples in Inner Tank (provided by CVA)**

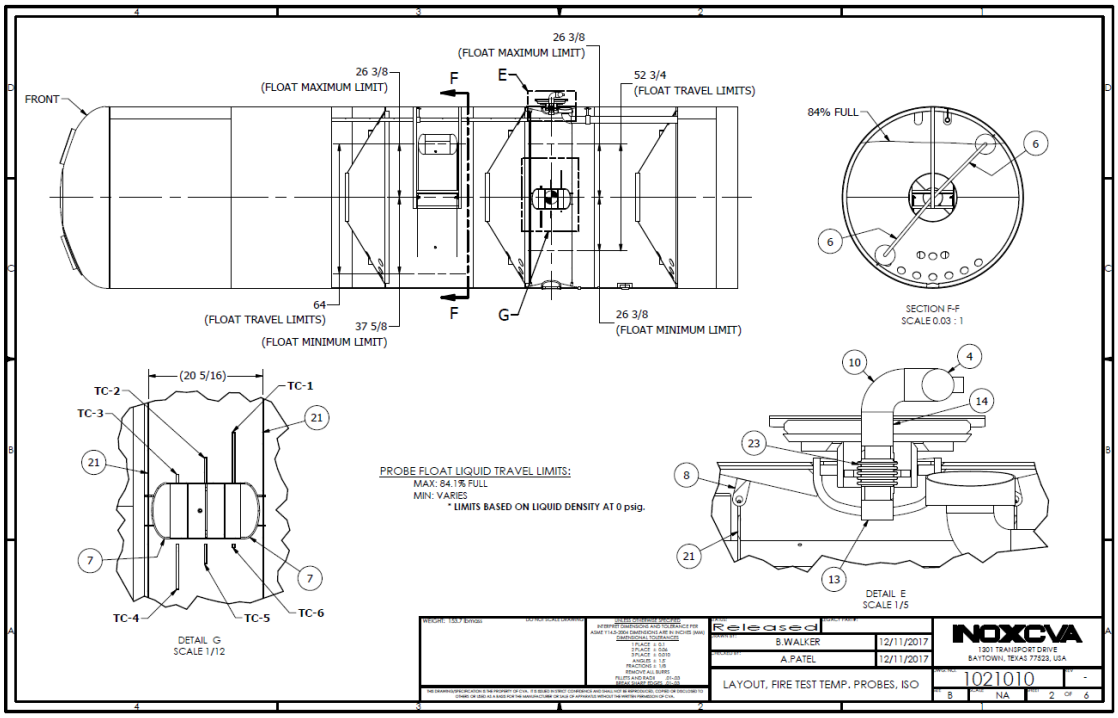


**Figure B-2. ISO Tank Showing Details for Central Floats and Top Outlet Connection for Wires (provided by CVA)**

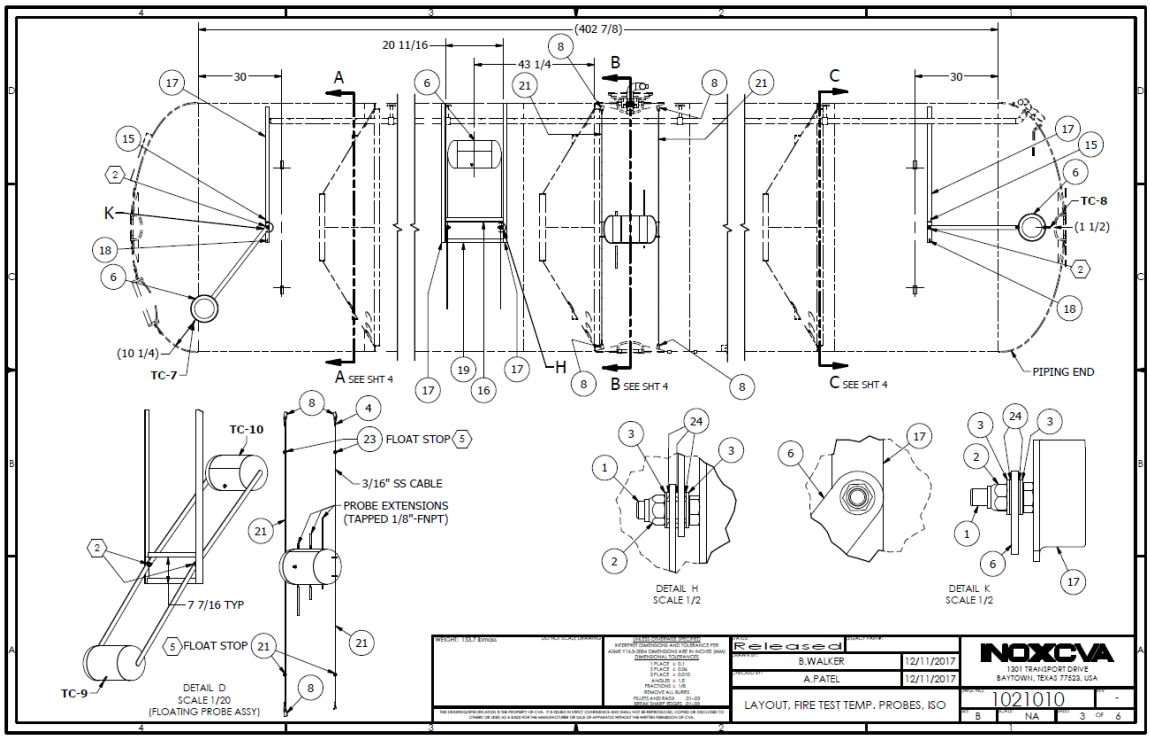


**Figure B-3. ISO Tank Showing Additional Details for Radial Floats at the End of the Tank (provided by CVA)**

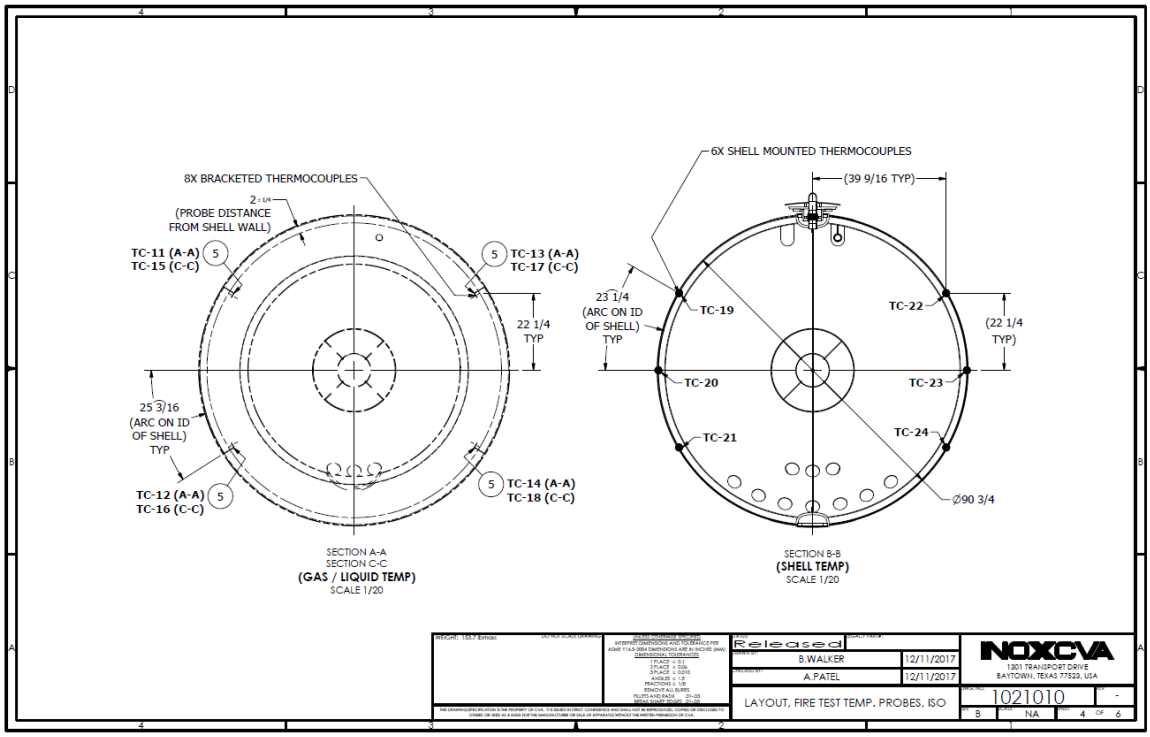


**Figure B-4. ISO Tank Showing Additional Details for Thermocouples Installed on Shell of Inner Tank (provided by CVA)**

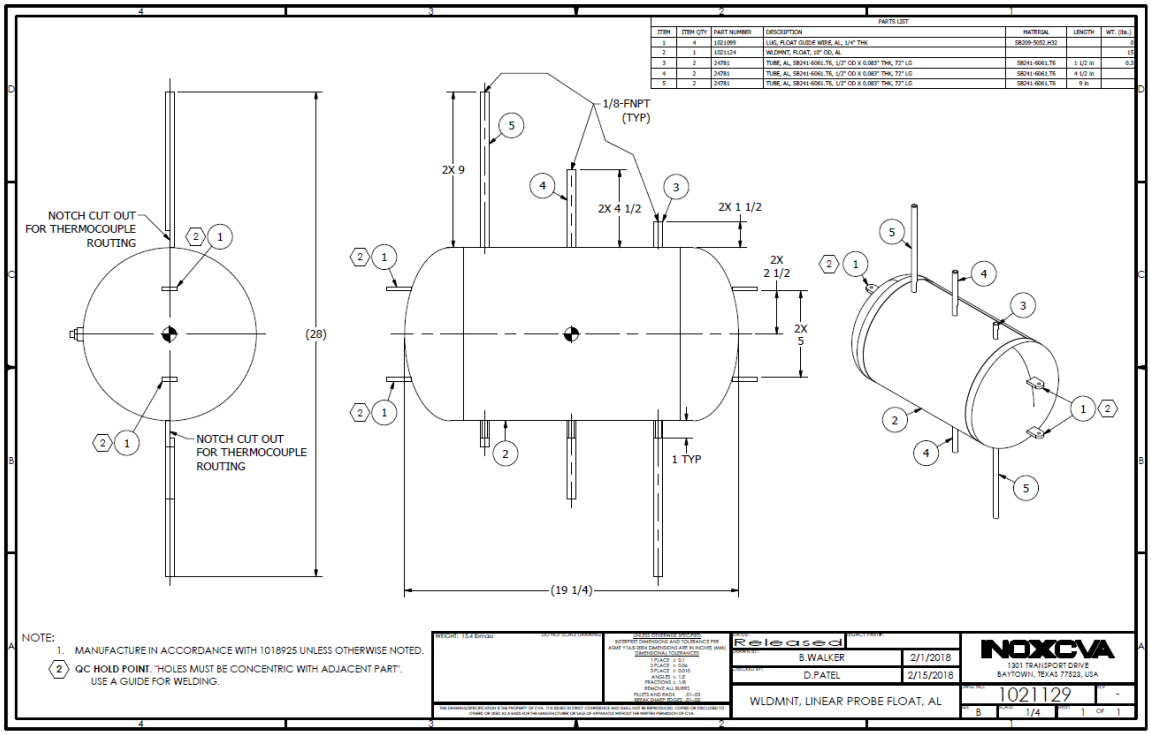


**Figure B-5. Additional Detailed Drawing of Central Float Design (provided by CVA)**

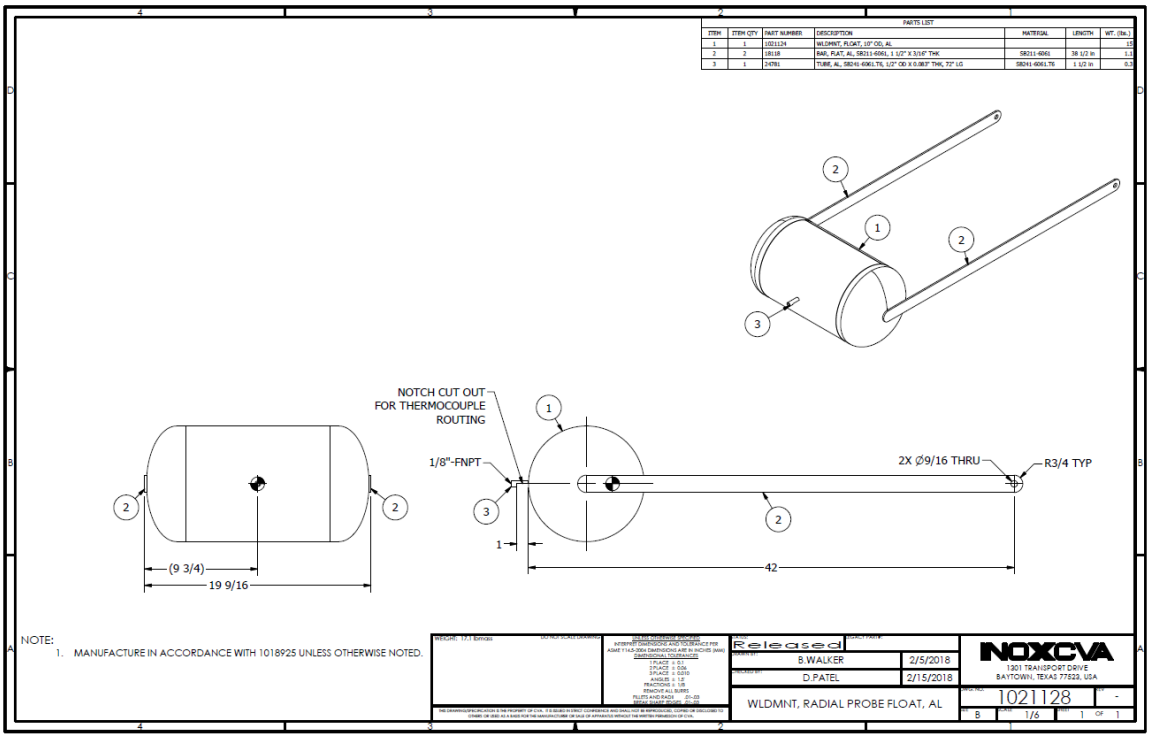


**Figure B-6. Additional Detailed Drawing of Radial Float Design (provided by CVA)**

## Abbreviations and Acronyms

| | |
|---|---|
| AAR | Association of American Railroads |
| BLEVE | Boiling Liquid Expanding Vapor Explosion |
| CFD | Computational Fluid Dynamics |
| CNG | Compressed Natural Gas |
| CVA | Cryogenic Vessel Alternatives, Inc. |
| DAQ | Data Acquisition System |
| DFT | Directional flame thermometer |
| DOT | Department of Transportation |
| FDS | Fire Dynamics Simulator |
| FE | Finite Element |
| FECR | Florida East Coast Railway |
| FRA | Federal Railroad Administration |
| FRC | Freidman Research Corporation |
| FTD | Fire Technology Department |
| GHG | Greenhouse Gas |
| HRRPUA | heat release rate per unit area |
| ISO | International Organization for Standardization |
| LN2 | Liquid Nitrogen |
| LNG | Liquefied Natural gas |
| LPG | Liquefied Petroleum Gas |
| OSHA | Occupational Safety and Health Administration |
| PRV | Pressure Relief Valve |
| SwRI | Southwest Research Institute |
| TAG | Technical advisory group |
| TC | Thermocouple |